

**FROM QUANTUM FIELD THEORY TO NANO-OPTICS :
REFRACTIVE PROPERTIES OF GRAPHENE IN A MEDIUM-STRONG EXTERNAL MAGNETIC FIELD**

O. Coquand ^{1 2}, B. Machet ^{3 4 5 6}

Abstract: 1-loop quantum corrections are shown to induce large effects on the refraction index n inside a graphene strip in the presence of an external magnetic field B orthogonal to it. To this purpose, we use the tools of Quantum Field Theory to calculate the photon propagator at 1-loop inside graphene in position space, which leads to an effective vacuum polarization in a brane-like theory of photons interacting with massless electrons at locations confined inside the thin strip (its longitudinal spread is considered to be infinite). The effects factorize into quantum ones, controlled by the value of B and that of the electromagnetic coupling α , and a “transmittance function” U in which the geometry of the sample and the resulting confinement of electrons play the major roles. We consider photons inside the visible spectrum and magnetic fields in the range 1-20 Teslas. At $B = 0$, quantum effects depend very weakly on α and n is essentially controlled by U ; we recover, then, an opacity for visible light of the same order of magnitude $\pi\alpha_{vac}$ as measured experimentally.

¹Ecole Normale Supérieure, 61 avenue du Président Wilson, F-94230 Cachan

²ocoquand@ens-cachan.fr

³Sorbonne Université, UPMC Univ Paris 06, UMR 7589, LP THE, F-75005, Paris, France

⁴CNRS, UMR 7589, LP THE, F-75005, Paris, France.

⁵Postal address: LP THE tour 13-14, 4^{ème} étage, UPMC Univ Paris 06, BP 126, 4 place Jussieu, F-75252 Paris Cedex 05 (France)

⁶machet@lpthe.jussieu.fr

Contents

1	Introduction	5
2	From the vacuum polarization to light-cone equations and to the refraction index	6
2.1	Conventions and setting	6
2.2	The modified Maxwell Lagrangian and the light-cone equations	7
2.3	The refractive index	8
3	Calculation of the 1-loop vacuum polarization $\Pi^{\mu\nu}(\hat{q}, B)$ in the presence of an external magnetic field B	8
3.1	The electron propagator in an external magnetic field	9
3.1.1	Expanding at “large” $B < \infty$	9
3.1.2	Our working approximation	10
3.2	Calculation and results	10
3.2.1	Performing the traces of γ matrices	10
3.2.2	Doing the integrations	10
3.2.3	Explicit expression of the vacuum polarization at 1-loop	12
3.2.4	Comments	12
4	The photon propagator in x-space and the effective vacuum polarization $\Pi_{eff}^{\mu\nu}$	12
4.1	The 1-loop photon propagator in position space	13
4.1.1	Standard QFT	13
4.1.2	The case of graphene electrons confined along z	14
4.1.3	The transmittance function $U(q, y_3)$. A choice of gauge.	15
4.1.4	Going to dimensionless variables	15
5	The light-cone equations and their solutions	16
5.1	Orders of magnitude	16
5.2	The light-cone equations	16
5.3	Calculating the transmittance V	17
5.4	Solving the light-cone equations for A_{\parallel}^{μ} and $n \in \mathbb{R} > \frac{1}{\sin \theta}$	17
5.4.1	Calculation of V	18
5.4.2	The imaginary parts of the light-cone equations	18
5.4.3	There is no non-trivial solution for A_{\perp}^{μ}	18
5.4.4	The light-cone equation for A_{\parallel}^{μ} and its solution	18
5.4.5	Graphical results and comments	19
5.4.6	The “leading” $n \sim \frac{1}{\sin \theta}$ behavior	20
5.5	The transition $\theta \rightarrow 0$	20
5.6	The quantum upper bound $n < n_{quant}$. The threshold at $B = B^m$	22

5.7	Reliability of the approximation $F(x) \approx \frac{1}{1-x}$ for the electron propagator	22
5.8	Going to $n \in \mathbb{C}$	22
5.8.1	The case of A_{\parallel}^{μ}	22
5.8.2	The “wall” for A_{\parallel}^{μ}	23
5.8.3	An estimate of the angle of transition θ_{min}	24
5.8.4	The case of A_{\perp}^{μ}	25
6	The case $B = 0$	26
6.1	The vacuum polarization $\Pi^{\mu\nu}$	26
6.2	The light-cone equation and the refractive index	27
6.3	Solutions for A_{\parallel}^{μ} with $n \in \mathbb{R}$	27
6.4	Solutions with $n \in \mathbb{C}$	28
6.4.1	There is no solution with $n_1 < \frac{1}{s_{\theta}}$	28
6.4.2	The solution with $n_1 > \frac{1}{s_{\theta}}$	28
6.5	The limit of very small θ ; absorption of visible light and experimental opacity	29
6.5.1	At small θ	29
6.5.2	At $\theta = 0$	30
7	Outlook and prospects	30
7.1	General remarks	30
7.2	Going below θ_{min} in the presence of B ; are there also solutions with a large absorption?	31
7.3	A bridge between Quantum Field Theory, quantum optics and nanophysics	32

List of Figures

1	\vec{B} is perpendicular to the graphene strip of width $2a$. The polarization vector $\vec{\epsilon}$, perpendicular to the momentum \vec{q} of the electromagnetic wave, is decomposed into $\vec{\epsilon}_{\parallel}$ in the (x, z) plane and $\vec{\epsilon}_{\perp}$ perpendicular to this plane.	7
2	The vacuum polarization $\Pi^{\mu\nu}$	8
3	The contour of integration for $B(q_0)$ and $C(q_0)$	11
4	The index $n \in \mathbb{R}$ for A_{\parallel}^{μ} as a function of θ . On the left we vary $\alpha = 1/137$ (<i>blue</i>), 1 (<i>purple</i>), 2 (<i>green</i>) at $\Upsilon = 10$; on the right we vary $\Upsilon = 5$ (<i>blue</i>), 10 (<i>purple</i>), 15 (<i>green</i>), 20 (<i>yellow</i>) at $\alpha = 1$. The lower (black) curves are $1/\sin \theta$	19
5	The imaginary part n_2 of the index n for A_{\parallel}^{μ} as a function of θ . On the left we vary $\alpha = 1/137$ (<i>blue</i>), 1 (<i>purple</i>), 2 (<i>green</i>) at $\Upsilon = 5$; on the right we vary $\Upsilon = 4$ (<i>blue</i>), 8 (<i>purple</i>), 12 (<i>green</i>) at $\alpha = 1$. The dashed curves on the right correspond to the rough approximation (81)	22
6	The imaginary part n_2 of index n for A_{\parallel}^{μ} as a function of u . We take $\alpha = 1$, $\eta = 5/1000$, and vary $\Upsilon = 4$ (<i>blue</i>), 8 (<i>purple</i>), 12 (<i>green</i>)	23
7	The index (n_1, n_2) for A_{\parallel}^{μ} at $\theta = \frac{\pi}{4}$ (left) and $\theta = \frac{\pi}{10}$ (right)	24
8	The index (n_1, n_2) for A_{\parallel}^{μ} at $\theta = \frac{\pi}{17}$. The right figure is an enlargement of the left one	24
9	The 2 types of real solutions of the light-cone equation for A_{\parallel}^{μ} as a function of θ when no external B is present. On the left $n > \frac{1}{s_{\theta}}$, on the right $n < \frac{1}{s_{\theta}}$. We vary $\alpha = 1/137$ (<i>blue</i>), 1 (<i>purple</i>), 1.5 (<i>green</i>), 2 (<i>yellow</i>). The black (\simeq blue) curves are $1/\sin \theta$	27
10	The real part n_1 (left) and imaginary part n_2 (right) of the solution n of the light-cone equation (90) for A_{\parallel}^{μ} in the absence of external B . The blue curves correspond to $\alpha = 1$, the purple curves to $\alpha = 1.5$ and the green curves to $\alpha = 2$. The black curve on the left is $n_1 = \frac{1}{s_{\theta}}$	28
11	n_2 as a function of θ for $\eta = \frac{2}{1000}$ (green) and $\eta = \frac{7}{1000}$ (brown), in the case $\alpha = 1.5$	29
12	Solutions of the real part (purple) and imaginary part (blue) of the light-cone equation (82) for A_{\parallel}^{μ} at $\theta = \frac{\pi}{17}$ in the presence of B . The black vertical line on the left corresponds to $n_1 = \frac{1}{s_{\theta}}$	32

1 Introduction

Very strong magnetic fields B are known to induce dramatic effects on the spectrum of hydrogen and on the critical number Z_c of atoms [1] [2]. However, the typical effects being $\mathcal{O}(\frac{e^3 B}{m_e})$, gigantic fields are needed, $\geq 10^{16}$ Gauss, which are out of reach on earth.

The property that the fine structure constant α in graphene largely exceeds 1 [3] instead of its vacuum value $\alpha_{vac} \simeq \frac{1}{137}$ was a sufficient motivation to investigate whether sizable effects could be obtained at lower cost in there.

While graphene in an external magnetic field is usually associated to the so-called “abnormal quantum hall effect” [3] [4], our results show that one can also expect optical effects for the visible spectrum and “reasonable” values of the magnetic field.

This work relies on the Schwinger formalism [5] [6] to write the propagator of the Dirac-like massless electrons inside graphene in an external magnetic field B perpendicular to the graphene strip, and on a calculation in position space of the photon propagator at 1-loop. This enables in particular to explicitly constrain the vertices of electrons with photons to stay confined inside the graphene strip ¹. So doing, we get an effective 1-loop vacuum polarization $\Pi_{eff}^{\mu\nu}$ that can be plugged in the light-cone equations derived according to the pioneering work of Tsai and Erber [7], and of Dittrich and Gies [8].

One of the salient features of the effective $\Pi_{eff}^{\mu\nu}$ is that it factorizes into the 1-loop $\Pi^{\mu\nu}$ calculated with the standard rules of Quantum Field Theory (QFT) in the presence of an external magnetic field, adapted of course to the case of the Hamiltonian for graphene at the Dirac points, times a universal function U which does not depend on the magnetic field, but only on the energy q_0 of the photon, of the relative penetration u inside the graphene strip (very weakly), and of its “geometry” (in a somewhat extended meaning). It is classical by nature and shares similarities with the so called “transmittance” function in optics or “transfer function” in electronics. The genuine $\Pi^{\mu\nu}$ concentrates all quantum effects and those of the magnetic field.

It is also a remarkable fact that, though electrons inside graphene correspond classically to massless $3 + 1$ Dirac electrons with a vanishing momentum p_3 along the direction of B , the quantum calculation of the photon propagator at 1-loop shows that the latter can nevertheless exchange momentum with virtual electrons in the direction of B as expected from quantum mechanics and their confinement inside the small width $2a$ of the graphene strip: the corresponding unavoidable “energy-momentum non-conservation” of photons along B is found indeed to be the quantum uncertainty \hbar/a on the electron momentum.

The effects that we describe only concern photons with “parallel” polarization (see [7]) (for transverse polarization, the only solution that we found to the light-cone equation is the trivial $n = 1$). The large value of the electromagnetic coupling turns out not to be only amplifying factor. That the massless Dirac electrons of graphene that interact with photons are confined inside a thin strip plays also a major role.

The effects of the confinement of electrons that arise add to the ones that have, for example, been investigated in [9] when the longitudinal size L of graphene is finite. Confinement conspires with the external magnetic field to produce macroscopic effects. The difference is that we are concerned here with the confinement in the “short” direction, the thickness $2a \approx 350 \text{ pm}$ of graphene, considering that its large direction L is like infinite ². This makes an intuitive physical interpretation much less easy since, now, no cyclotron radius can eventually reach the (longitudinal) size of the graphene strip.

¹Sometimes we write abusively about the confinement of electrons, but we always mean that the vertices at which they interact with photons lie inside graphene and are therefore confined in the z direction between $-a$ and $+a$.

²The cyclotron radius $\ell = \sqrt{\frac{\hbar}{eB}}$ is $\ell \approx 8.1 \cdot 10^{-9} \text{ m}$ at $B = 10 \text{ T}$.

The refractive index $n = n_1 + i n_2$ is found to essentially depend on α , on the angle of incidence θ , and on the ratio $\Upsilon = \frac{\sqrt{2eB}}{q_0}$. In the absence of any external B , its dependence on the electromagnetic coupling fades away, and it is mainly constrained by the sole property that electrons are confined.

A transition occurs at small angle of incidence $\theta_{min} \sim \frac{1}{\Upsilon}$: no solution with $|n_2| \ll n_1$ to the light-cone equation exists anymore for $\theta < \theta_{min}$. There are hints that the system goes brutally to a regime with large index/absorption. The identification of the corresponding solutions however requires more elaborate numerical techniques, which will be the object of a subsequent work.

That the final results differ from what would be obtained from QED_{2+1} is expected since the gauge field, unlike the electrons, lives in $3 + 1$ dimension and the framework of our calculations is more a “brane-like” picture for graphene.

Our calculations are made in the limit of a “medium-strong” B , in the sense that $\sqrt{2eB} \gg q_0$, and are only valid at this limit such that, in particular, the case $B = 0$ is not directly accessible. This is why we have performed a special calculation for $B = 0$ the end of the study. B is however not considered to be “infinite” like in [1] [2] [10]. They also require $aq_0 \ll 1$, in which $2a$ is the thickness of the graphene strip. This last approximation guarantees to stay in the linear part of the electron spectrum close to the Dirac point, which is an essential ingredient to use a “Dirac-like” effective Hamiltonian [3]. We are concerned with photons in the visible spectrum, which sets us very far from geometrical optics³, and limit B , for the sake of experimental feasibility, to 20 Teslas.

Our results are summarized in the 2 plots of Figure 4.

The last section is dedicated to the case when no external magnetic field is present. We show in this case that no θ_{min} exists and that, instead, when the angle of incidence gets smaller and smaller, the refraction index n goes continuously from “quasi-real” values to complex values with larger n_1 and n_2 . At very small values of θ , we recover an opacity of the same order of magnitude as the one measured experimentally [11].

The literature dedicated to graphene is enormous and we cannot unfortunately pay a tribute to the whole of it. We only make few citations, but the reader can find, in particular inside the reviews articles, references to most of the important works.

2 From the vacuum polarization to light-cone equations and to the refraction index

2.1 Conventions and setting

Let us follow Tsai-Erber [7]. \vec{B} is $\parallel z$, the \vec{q} of the propagating photon (plane wave) is chosen to lie in the (x, z) plane. See Fig. 1.

We shall call θ the “angle of incidence”; the reader should keep in mind that, since we are concerned with the propagation of light *inside* graphene, θ is the angle of incidence of light *inside this medium*.

The polarization vector $\vec{\epsilon}$ is decomposed into $\vec{\epsilon}_{\parallel}$ and $\vec{\epsilon}_{\perp}$, both orthogonal to \vec{q} . $\vec{\epsilon}_{\perp} \parallel y$ and $\vec{\epsilon}_{\parallel}$ is in the (x, z) plane. If we call θ the angle (\vec{B}, \vec{q}) , $\vec{\epsilon}_{\parallel} = -\cos \theta \vec{i} + \sin \theta \vec{k}$, while $\vec{\epsilon}_{\perp} = \vec{j}$. One has $\vec{q} = |\vec{q}| (\sin \theta \vec{i} + \cos \theta \vec{k})$. We shall call $\vec{\epsilon}_{\parallel}$ “parallel polarization” and $\vec{\epsilon}_{\perp}$ “transverse polarization”. It must be noticed that, at normal incidence $\theta = 0$, there is no longer a plane (\vec{q}, B) such that these 2 polarizations can no longer be distinguished.

We shall in the following use “hatted” letters for vectors living in the Lorentz subspace $(0, 1, 2)$. For example

$$\hat{q} = (q^0, q^1, q^2), \quad q = (\hat{q}, q_3) = (q_0, q_1, q_2, q_3). \quad (1)$$

³The corresponding wavelengths are indeed roughly 3 orders of magnitude larger than the thickness of graphene.

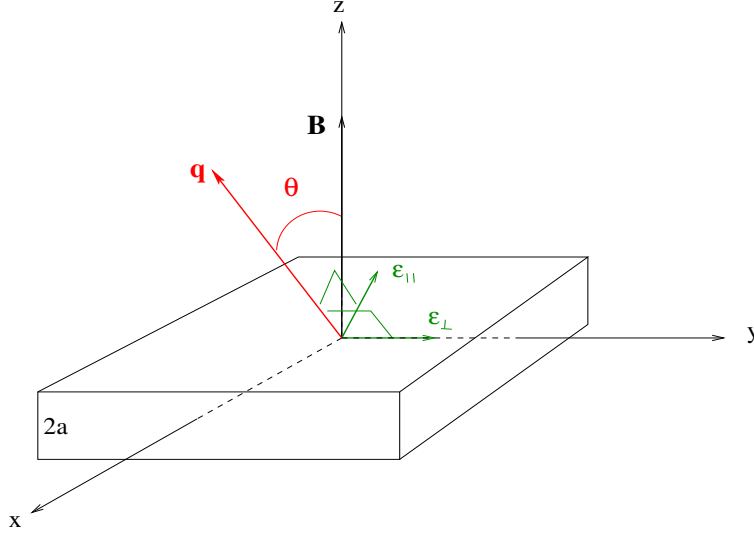


Figure 1: \vec{B} is perpendicular to the graphene strip of width $2a$. The polarization vector $\vec{\epsilon}$, perpendicular to the momentum \vec{q} of the electromagnetic wave, is decomposed into $\vec{\epsilon}_{\parallel}$ in the (x, z) plane and $\vec{\epsilon}_{\perp}$ perpendicular to this plane.

2.2 The modified Maxwell Lagrangian and the light-cone equations

Taking into account the contribution of vacuum polarization, the Maxwell Lagrangian gets modified to [8]

$$\mathcal{L}(x) = -\frac{1}{4}F_{\mu\nu}(x)F^{\mu\nu}(x) - \frac{1}{2} \int d^4y A^{\mu}(x)\Pi_{\mu\nu}(x, y, B)A^{\nu}(y), \quad (2)$$

from which one gets the Euler-Lagrange equation

$$\left(g_{\mu\nu} q^2 - q_{\mu}q_{\nu} + \Pi_{\mu\nu}(q, B)\right)A^{\nu}(q) = 0. \quad (3)$$

Left-multiplying (3) with

$$A^{\mu} = \alpha\epsilon_{\perp}^{\mu} + \beta\epsilon_{\parallel}^{\mu}, \quad (4)$$

yields ⁴

$$\begin{aligned} &(\alpha\epsilon_{\perp}^{\mu} + \beta\epsilon_{\parallel}^{\mu})\left(g_{\mu\nu} q^2 - q_{\mu}q_{\nu} + \Pi_{\mu\nu}(q, B)\right)(\alpha\epsilon_{\perp}^{\nu} + \beta\epsilon_{\parallel}^{\nu}) = 0, \\ &\epsilon_{\perp}^{\mu} = (0, 0, 1, 0), \quad \epsilon_{\parallel}^{\mu} = (0, -c_{\theta}, 0, s_{\theta}), \quad c_{\theta} \equiv \cos \theta, \quad s_{\theta} \equiv \sin \theta. \end{aligned} \quad (5)$$

We shall identify $\Pi^{\mu\nu}$ with the *effective polarization* inside graphene $\Pi_{eff}^{\mu\nu}$ that we shall calculate in section 4 and therefore consider in the following, instead of (3), the Euler-Lagrange equation

$$\left(g^{\mu\nu} q^2 - q^{\mu}q^{\nu} + \Pi_{eff}^{\mu\nu}(q, B)\right)A_{\nu}(q) = 0. \quad (6)$$

As we shall see there, $\Pi_{eff}^{03} = 0 = \Pi_{eff}^{13} = \Pi_{eff}^{23}$, such that we shall be concerned with the simplified light-cone equation

$$(\alpha^2 + \beta^2)q^2 + (\alpha^2\Pi_{eff}^{22}(q, B) + \beta^2(c_{\theta}^2\Pi_{eff}^{11}(q, B) + s_{\theta}^2\Pi_{eff}^{33}(q, B)) + 2\alpha\beta c_{\theta}\Pi_{eff}^{12}(q, B)) = 0. \quad (7)$$

⁴When $\Pi_{\mu\nu}$ is not present, the only non-vanishing elements are “diagonal”, $\epsilon_{\perp}^{\mu}(g_{\mu\nu} q^2 - q_{\mu}q_{\nu})\epsilon_{\perp}^{\nu} = q^2 = \epsilon_{\parallel}^{\mu}(g_{\mu\nu} q^2 - q_{\mu}q_{\nu})\epsilon_{\parallel}^{\nu}$, which yields $A^{\mu}(g_{\mu\nu} q^2 - q_{\mu}q_{\nu})A^{\nu} = (\alpha^2 + \beta^2)q^2$, and, accordingly, the customary light-cone condition $q^2 = 0 \equiv q_0^2 - \vec{q}^2$. If $\Pi_{\mu\nu}$ is transverse $\Pi_{\mu\nu} = (g_{\mu\nu}q^2 - q_{\mu}q_{\nu})\Pi(q^2)$, the light-cone condition is $(\alpha^2 + \beta^2)q^2(1 + \Pi(q^2)) = 0$, that is, as usual, $q^2 = 0$.

\vec{q} has been furthermore chosen to lie in the (x, z) plane, so $q_2 = 0$, which entails (see (32)) $\Pi_{eff}^{02} = 0 = \Pi_{eff}^{20}, \Pi_{eff}^{12} = 0 = \Pi_{eff}^{21}$, and the light-cone relation finally shrinks to

$$(\alpha^2 + \beta^2)q^2 + (\alpha^2 \Pi_{eff}^{22}(q, B) + \beta^2 (c_\theta^2 \Pi_{eff}^{11}(q, B) + s_\theta^2 \Pi_{eff}^{33}(q, B))) = 0. \quad (8)$$

Depending of the polarization of the photon, there are accordingly 2 different light-cone relations:

- for $A_\perp^\mu(q_0, q_1, 0, q_3)$, $\alpha = 1, \beta = 0$,

$$q^2 + \Pi_{eff}^{22}(q, B) = 0; \quad (9)$$

- for $A_\parallel^\mu(q_0, q_1, 0, q_3)$, $\alpha = 0, \beta = 1$,

$$q^2 + (c_\theta^2 \Pi_{eff}^{11}(q, B) + s_\theta^2 \Pi_{eff}^{33}(q, B)) = 0. \quad (10)$$

One of the main features of (10) is the occurrence of Π_{eff}^{33} , which would not be there in QED_{2+1} . We shall see later that this term plays an important role.

A remark is due concerning eq. (3). Its derivation from the effective Lagrangian (2) relies on the property that $\Pi_{\mu\nu}(x, y)$ is in reality a function of $(x - y)$ only. This is however not the case for $\Pi_{eff}^{\mu\nu}$ which, as we shall see, depends indeed on $(\hat{x} - \hat{y})$ but individually on x_3 and y_3 (see the first remark at the end of subsection 4.1.2). Once the dependence on $(x_3 - y_3)$ has been extracted, there is a left-over dependence on y_3 , which finally yields for our results the dependence of the refraction index on $u = \frac{y_3}{a} \in [-1, +1]$. We shall see however that this dependence is always extremely weak, and we consider therefore the Euler-Lagrange equation (6) to be valid to a very good approximation.

2.3 The refractive index

We define it in a standard way by

$$n = \frac{|\vec{q}|}{q_0}. \quad (11)$$

In practice, $\Pi_{eff}^{\mu\nu}$ is not only a function of q and B , but of the angle of incidence θ and of the relative depth u inside the graphene strip, $u \in [-1, +1]$. The light-cone equations therefore translate into relations $n = n(\theta, B, q_0, u)$ that we will write explicitly after calculating $\Pi^{\mu\nu}$ and $\Pi_{eff}^{\mu\nu}$.

3 Calculation of the 1-loop vacuum polarization $\Pi^{\mu\nu}(\hat{q}, B)$ in the presence of an external magnetic field B

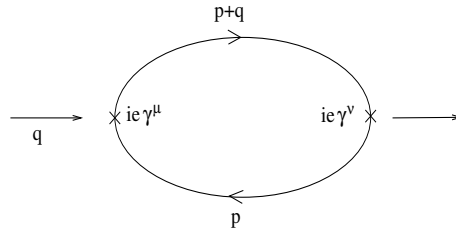


Figure 2: The vacuum polarization $\Pi^{\mu\nu}$

It is given by

$$i\Pi^{\mu\nu}(\hat{q}, B) = +e^2 \int_{-\infty}^{+\infty} \frac{d^3 \hat{p}}{(2\pi)^3} \text{Tr} [\gamma^\mu G(\hat{p}, B) \gamma^\nu G(\hat{p} + \hat{q}, B)], \quad (12)$$

in which $G(\hat{p}, B)$ is the propagator of a massless Dirac electron obtained from the Hamiltonian of graphene at the Dirac points, making use of the formalism of Schwinger [5][12] to account for the external magnetic field B .

3.1 The electron propagator in an external magnetic field

Following Schwinger ([5], eqs. 2.7 to 2.10), we define the electron propagator as

$$G(x, y) = i \langle (\psi(x) \bar{\psi}(y))_+ \rangle \Theta(x - y). \quad (13)$$

The graphene at the Dirac points is described (see for example [3] [4]) by a Hamiltonian which is exactly Dirac in 4 dimensions but with $m_e = 0$ and $p_3 = 0$ (and the γ matrices taken in the chiral representation).

The propagator of an electron inside graphene will accordingly be taken to be [5][12]⁵

$$G(\hat{p}, B) = \int_0^\infty d\tau \exp \left[-\tau \left((-p_0^2) + \frac{\tanh(e\tau B)}{e\tau B} (p_1^2 + p_2^2) \right) \right] \left((\gamma^0 p^0) (1 - i\gamma^1 \gamma^2 \tanh(e\tau B)) - \frac{\gamma_1 p_1 + \gamma_2 p_2}{\cosh^2(e\tau B)} \right), \quad (14)$$

which only depends on $\hat{p} = (p_0, p_1, p_2)$ and B .

3.1.1 Expanding at “large” $B < \infty$

At the limit $B \rightarrow \infty$ ⁶, (14) becomes

$$G(\hat{p}, B) \xrightarrow{B \rightarrow \infty} -e^{-\frac{p_\perp^2}{eB}} \frac{\gamma^0 p^0}{p_0^2} (1 - i\gamma^1 \gamma^2), \quad p_\perp^2 = p_1^2 + p_2^2. \quad (15)$$

We shall in this work go one step further in the expansion of G at large B : we keep the first subleading terms in the expansions of $\tanh(\tau eB)$ and $\cosh(\tau eB)$ of (14)⁷:

$$\tanh(\tau eB) \approx 1 - 2e^{-2\tau eB}, \quad \cosh^2(\tau eB) \approx \frac{e^{2\tau eB} + 2}{4} \Rightarrow \frac{1}{\cosh^2(\tau eB)} \approx \frac{4e^{-2\tau eB}}{1 + 2e^{-2\tau eB}}. \quad (16)$$

This gives (we note $(\gamma p)_\perp = \gamma_1 p_1 + \gamma_2 p_2$), still for graphene,

$$G(\hat{p}, B) \approx \int_0^\infty d\tau e^{-\tau(-p_0^2)} e^{-\frac{p_\perp^2}{eB}(1-2e^{-2\tau eB})} (\gamma^0 p^0) (1 - i\gamma^1 \gamma^2 (1 - 2e^{-2\tau eB})) - 4(\gamma p)_\perp \int_0^\infty d\tau e^{-2\tau eB} \frac{1}{1 + 2e^{-2\tau eB}} e^{-\tau(-p_0^2)} e^{-\frac{p_\perp^2}{eB}(1+2e^{-2\tau eB})}. \quad (17)$$

We shall further approximate $e^{-\frac{p_\perp^2}{eB}(1-2e^{-2\tau eB})} \approx e^{-\frac{p_\perp^2}{eB}}$, which can be seen to be legitimate because the exact integration yields subleading corrections $\propto 1/(eB)^2$, while the ones that we keep are $\propto 1/eB$. This gives

$$G(\hat{p}, B) \approx e^{-\frac{p_\perp^2}{eB}} \left(-\frac{\gamma^0 p^0}{p_0^2} (1 - i\gamma^1 \gamma^2) + 2 \frac{\gamma^0 p^0}{p_0^2 - 2eB} (-i\gamma^1 \gamma^2) \right) - 4(\gamma p)_\perp e^{-\frac{p_\perp^2}{eB}} \int_0^\infty d\tau \frac{1}{1 + 2e^{-2\tau eB}} e^{-\tau(-p_0^2 + 2eB)}. \quad (18)$$

One has

$$\int_0^\infty d\tau \frac{1}{1 + 2e^{-2\tau eB}} e^{-\tau(-p_0^2 + 2eB)} = (-2)^{-1 + \frac{p_0^2}{2eB}} \frac{\beta(-2, 1 - \frac{p_0^2}{2eB}, 0)}{2eB}, \quad (19)$$

⁵The expression (14) is obtained after going from the real proper-time s of Schwinger to $\tau = is$ and switching to conventions for the Dirac matrices and for the metric of space $(+, -, -, -)$ which are more usual today [13].

⁶One considers then that $e\tau B$ also $\rightarrow \infty$, in which case, in (14) $\tanh e\tau B \rightarrow 1$, $\cosh e\tau B \rightarrow \infty$. This is only acceptable at $\tau \neq 0$, but Schwinger's prescription is that the integration over the proper time has to be made last.

⁷This approximation does not allow later to take the limit $B \rightarrow 0$ since, for example, it yields $\tanh(\tau eB) \rightarrow -1$ instead of 0 and $\cosh^2(\tau eB) \rightarrow 3/4$ instead of 1.

such that (18) rewrites

$$G(\hat{p}, B) = -e^{-\frac{p_0^2}{eB}} \left(\frac{\gamma^0}{p^0} \left(1 + i\gamma_1\gamma_2 \frac{p_0^2 + 2eB}{p_0^2 - 2eB} \right) + 4 \frac{p_1\gamma_1 + p_2\gamma_2}{2eB} F\left(\frac{p_0^2}{2eB}\right) \right), \quad F(x) = (-2)^{(-1+x)} \beta(-2, 1-x, 0), \quad (20)$$

in which β is the incomplete beta function.

When $B < \infty$, corrections arise with respect to (15), which exhibit in particular poles at $p_0^2 = 2eB$ (first and 2nd term) and also $p_0^2 = 2n eB, n = 1, 2 \dots$ (second term) ⁸.

3.1.2 Our working approximation

The expression (20) is still not very simple to use. This is why we shall further approximate $F(x)$ and take

$$F(x) \approx \frac{1}{1-x}, \quad (21)$$

which amounts to only select, in there, the pole at $p_0^2 = 2eB$ and neglect the other poles. This approximation is reasonable in the vicinity of this pole, for $0 \leq x \leq 1.5$, that is $0 \leq p_0^2 \leq 1.5 \times (2eB)$, low energy (massless) electrons. It will be discussed more in subsection 5.7 in which we show that the approximation is valid for electrons with energy $p_0 \leq 10 eV$ at the weakest magnetic fields $B = 1 T$ that we consider..

We shall accordingly take

$$G(\hat{p}, B) \approx -e^{-\frac{p_0^2}{eB}} \left[\frac{\gamma^0}{p^0} \left(1 + i\gamma_1\gamma_2 \frac{p_0^2 + 2eB}{p_0^2 - 2eB} \right) - 4 \frac{p_1\gamma_1 + p_2\gamma_2}{p_0^2 - 2eB} \right]. \quad (22)$$

This leads to expressions much easier to handle, and enables to go a long way analytically.

3.2 Calculation and results

There are 2 steps in the calculation. First one has to perform the traces on the Dirac γ matrices, then do explicitly the integration over the loop variable \hat{p} .

3.2.1 Performing the traces of γ matrices

This step already yields

$$\Pi^{i3} = 0 = \Pi^{3i}, \quad i = 0, 1, 2. \quad (23)$$

3.2.2 Doing the integrations

Details of the calculation will be given somewhere else. We just want here to present its main steps, taking the example of Π^{00} . After doing the traces, one gets

$$i\Pi^{00}(\hat{q}, B) = 4e^2 \int_{-\infty}^{+\infty} \frac{dp_0 dp_1 dp_2}{(2\pi)^3} e^{-p_0^2/eB} e^{-(p_1+q_1)^2/eB} \left(\frac{1}{p_0} \frac{1}{p_0 + q_0} + \frac{1}{p_0} \frac{p_0^2 + 2eB}{p_0^2 - 2eB} \frac{1}{p_0 + q_0} \frac{(p_0 + q_0)^2 + 2eB}{(p_0 + q_0)^2 - 2eB} + 16 \frac{p_1(p_1 + q_1) + p_2(p_2 + q_2)}{(p_0^2 - 2eB)((p_0 + q_0)^2 - 2eB)} \right), \quad (24)$$

⁸If we do not work explicitly for graphene, one finds that the electron mass squared m_e^2 gets replaced by $m_e^2 + 2n eB$ in the presence of B .

which decomposes into

$$\begin{aligned}
i\Pi^{00}(\hat{q}, B) &= I(\hat{q}, B) + J(\hat{q}, B) + K(\hat{q}, B), \\
I(\hat{q}, B) &= 4e^2 \int_{-\infty}^{+\infty} \frac{dp_0 dp_1 dp_2}{(2\pi)^3} e^{-p_\perp^2/eB} e^{-(p+q)_\perp^2/eB} \frac{1}{p_0} \frac{1}{p_0 + q_0}, \\
J(\hat{q}, B) &= 4e^2 \int_{-\infty}^{+\infty} \frac{dp_0 dp_1 dp_2}{(2\pi)^3} e^{-p_\perp^2/eB} e^{-(p+q)_\perp^2/eB} \frac{1}{p_0} \frac{p_0^2 + 2eB}{p_0^2 - 2eB} \frac{1}{p_0 + q_0} \frac{(p_0 + q_0)^2 + 2eB}{(p_0 + q_0)^2 - 2eB}, \\
K(\hat{q}, B) &= 4e^2 \int_{-\infty}^{+\infty} \frac{dp_0 dp_1 dp_2}{(2\pi)^3} e^{-p_\perp^2/eB} e^{-(p+q)_\perp^2/eB} 16 \frac{p_1(p_1 + q_1) + p_2(p_2 + q_2)}{(p_0^2 - 2eB)((p_0 + q_0)^2 - 2eB)}.
\end{aligned} \tag{25}$$

It is then convenient to introduce

$$\begin{aligned}
B(q_0) &= \int_{-\infty}^{+\infty} dp_0 \frac{1}{p_0} \frac{1}{p_0 + q_0}, \\
C(q_0, B) &= \int_{-\infty}^{+\infty} dp_0 \frac{1}{p_0} \frac{p_0^2 + 2eB}{p_0^2 - 2eB} \frac{1}{p_0 + q_0} \frac{(p_0 + q_0)^2 + 2eB}{(p_0 + q_0)^2 - 2eB}, \\
D(q_0, B) &= \int_{-\infty}^{+\infty} dp_0 \frac{1}{(p_0^2 - 2eB)((p_0 + q_0)^2 - 2eB)},
\end{aligned} \tag{26}$$

such that, integrating over the transverse degrees of freedom p_1, p_2 , one gets

$$\begin{aligned}
I(\hat{q}, B) &= \frac{\alpha}{\pi} eB e^{-q_\perp^2/2eB} B(q_0), \\
J(\hat{q}, B) &= \frac{\alpha}{\pi} eB e^{-q_\perp^2/2eB} C(q_0, B), \\
K(\hat{q}, B) &= \frac{8\alpha}{\pi} eB e^{-q_\perp^2/2eB} (eB - q_\perp^2) D(q_0, B).
\end{aligned} \tag{27}$$

“Massless” and ambiguous integrals of the type $\int_{-\infty}^{+\infty} d\sigma \frac{f(\sigma)}{\sigma}$ occurring in $B(q_0), C(q_0, B), D(q_0, B)$ are replaced, using the customary $+i\varepsilon$ prescription for the poles of propagators in QFT dictated by causality, with

$$\lim_{\varepsilon \rightarrow 0^+} \int_{-\infty}^{+\infty} d\sigma \frac{f(\sigma)}{\sigma + i\varepsilon} = -i\pi f(0) + \lim_{\varepsilon \rightarrow 0^+} \int_{|\sigma| > \varepsilon} \frac{f(\sigma)}{\sigma}, \tag{28}$$

which are just Cauchy integrals. This is nothing more than the Sokhotski-Plemelj theorem [14] :

$$\lim_{\varepsilon \rightarrow 0^+} \int_{-\infty}^{\infty} \frac{f(x)}{x \pm i\varepsilon} dx = \mp i\pi f(0) + \lim_{\varepsilon \rightarrow 0^+} \int_{|x| > \varepsilon} \frac{f(x)}{x} dx. \tag{29}$$

It is easy to also check that the same result can be obtained, after setting the $+i\varepsilon$ prescription, by integrating on the contour described on Fig.3. There, the 2 small 1/2 circles around the poles have radii that $\rightarrow 0$. The large 1/2 circle has infinite radius.

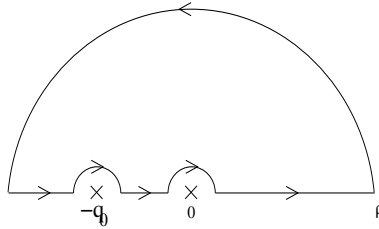


Figure 3: The contour of integration for $B(q_0)$ and $C(q_0)$

This also amounts, for the poles “on the real axis”, to evaluating $i\pi \sum \text{residues}$, that is 1/2 of what one would get if the poles were not on the real axis but inside the contour of integration. The other poles that lie inside the contour of integration are dealt with as usual by $2i\pi \times$ their residues.

So doing, one gets

$$\begin{aligned} B(q_0) &= 0 = C(q_0, B), \\ D(q_0, B) &= 2i\pi(-) \frac{1}{\sqrt{2eB}} \frac{1}{q_0^2 - 8eB}, \end{aligned} \quad (30)$$

leading finally to

$$I = 0 = J, \quad K(\hat{q}, B) = i \frac{2e^2}{\pi} e^{-\frac{q_\perp^2}{2eB}} \sqrt{2eB} \frac{eB - q_\perp^2}{q_0^2 - 8eB}, \quad (31)$$

and, for $\Pi^{00}(\hat{q}, B)$, to the first line of the set of equations (32).

After all integrals have been calculated by this technique, one gets the following results.

3.2.3 Explicit expression of the vacuum polarization at 1-loop

$$\begin{aligned} i\Pi^{00}(\hat{q}, B) &= 4i\alpha \sqrt{2eB} e^{-\frac{q_1^2 + q_2^2}{2eB}} \frac{2eB - 2(q_1^2 + q_2^2)}{q_0^2 - 4(2eB)} \xrightarrow{B \rightarrow \infty} -i\alpha \sqrt{2eB} e^{-\frac{q_1^2 + q_2^2}{2eB}}, \\ i\Pi^{11}(\hat{q}, B) &= 4i\alpha e^{-\frac{q_1^2 + q_2^2}{2eB}} \sqrt{2eB} \frac{q_1^2 - q_2^2}{q_0^2 - 4(2eB)} \xrightarrow{B \rightarrow \infty} i\alpha e^{-\frac{q_1^2 + q_2^2}{2eB}} \frac{q_1^2 - q_2^2}{\sqrt{2eB}}, \\ i\Pi^{22}(\hat{q}, B) &= -i\Pi^{11}(\hat{q}, B), \\ i\Pi^{01}(\hat{q}, B) &= 2i\alpha e^{-\frac{q_1^2 + q_2^2}{2eB}} q_1 q_0 \frac{\sqrt{2eB}}{q_0^2 - 2eB} \xrightarrow{B \rightarrow \infty} -i\alpha e^{-\frac{q_1^2 + q_2^2}{2eB}} \frac{q_1 q_0}{\sqrt{2eB}}, \\ i\Pi^{02}(\hat{q}, B) &= 2i\alpha e^{-\frac{q_1^2 + q_2^2}{2eB}} q_2 q_0 \frac{\sqrt{2eB}}{q_0^2 - 2eB} \xrightarrow{B \rightarrow \infty} -i\alpha e^{-\frac{q_1^2 + q_2^2}{2eB}} \frac{q_2 q_0}{\sqrt{2eB}}, \\ i\Pi^{12}(\hat{q}, B) &= -16\alpha q_1 q_2 e^{-\frac{q_1^2 + q_2^2}{2eB}} \frac{\sqrt{2eB}}{q_0^2 - 4(2eB)} \xrightarrow{B \rightarrow \infty} 4\alpha e^{-\frac{q_1^2 + q_2^2}{2eB}} \frac{q_1 q_2}{\sqrt{2eB}}, \\ i\Pi^{33}(\hat{q}, B) &= -i\Pi^{00}(\hat{q}, B), \\ i\Pi^{03}(\hat{q}, B) &= 0, \quad i\Pi^{13}(\hat{q}, B) = 0, \quad i\Pi^{23}(\hat{q}, B) = 0. \end{aligned} \quad (32)$$

3.2.4 Comments

- $\Pi^{00} = -\Pi^{33}$ are the only 2 components that do not vanish when $B \rightarrow \infty$ nor when $\theta \rightarrow 0$.
- The formula (22) of [10] taken at $m_e = 0$ yields $\Pi^{33} = -\Pi^{00}$; we get the same relation; it also yields $\Pi^{03} \propto \text{Tr}((k - q)_3 k_0 + (k - q)_0 k_3)$ such that, at $k_3 = 0 = (k - q)_3$ it yields 0 like we get.
- Transversality is broken since we do not have $q_\mu \Pi^{\mu\nu}(q) = 0$. At the opposite the general formula (34) in Tsai-Erber [7] for the vacuum polarization in magnetic field is shown in their eq. (36) to satisfy gauge invariance. In [10] the transversality conditions reduce to $q^0 \Pi_{03} + q^3 \Pi_{33} = 0 = q^0 \Pi_{00} + q^3 \Pi_{30}$, the other relations being automatically satisfied. Now, as can be easily checked in there, at $k_3 = 0 = (k - q)_3$, $\Pi_{03} = 0 = \Pi_{30}$, $\Pi_{33} \neq 0$, $\Pi_{00} \neq 0$, and the transversality conditions, which reduce to $q^3 \Pi_{33} = 0 = q^0 \Pi_{00}$ can non longer be satisfied either (unless $q_3 = 0 = q_0$). So, restraining the electrons to have a vanishing momentum along the direction of B breaks “gauge invariance”.

4 The photon propagator in x -space and the effective vacuum polarization $\Pi_{eff}^{\mu\nu}$

The vacuum polarization that needs to be introduced inside the light-cone equations (9,10) is not $\Pi^{\mu\nu}(\hat{q}, B)$ computed in section 3 above, but the effective $\Pi_{eff}^{\mu\nu}(\hat{q}, q_3, \frac{y_3}{a}, B)$ obtained by calculating the photon propagator in position-space, while confining, at the 2 vertices $\gamma e^+ e^-$, the corresponding z 's to lie inside graphene, $z \in [-a, a]$ ($2a$ is the graphene width).

The effective polarization writes $\Pi_{eff}^{\mu\nu}(\hat{q}, q_3, \frac{y_3}{a}, B) = \frac{1}{\pi^2} \Pi^{\mu\nu}(\hat{q}, B) U(\hat{q}, q_3, \frac{y_3}{a})$ in which U is a universal function that does not depend on the magnetic field and that we also encounter when dealing with the case of no external B . It is the Fourier transform of the product of 2 functions: the first, $\frac{\sin ak_3}{ak_3}$, is the Fourier transform of the “gate function” corresponding to the graphene strip along z ; the second carries the remaining information attached to the confinement of electrons. Its analytical properties inside the complex plane control in particular the “leading” $\frac{1}{\sin \theta}$ behavior of the refraction index inside graphene, where θ is the angle of incidence inside the graphene strip (see subsection 2.1). The integration variable of this transformation is k_3 , the difference between the momenta along B of the outgoing and incoming photons (see below).

This factorization can be traced back to the fact that $\Pi^{\mu\nu}$ does not depend on q_3 , for the simple reason that the Hamiltonian of electrons at the Dirac points inside graphene has $p_3 = 0$. An example of how factors combine is the following. $\Pi_{eff}^{\mu\nu}$ still includes an integration on p_3 (the component along B of the momentum of the virtual electron inside graphene). Like $\Pi^{\mu\nu}(\hat{q}, B)$, this integral factors out. Since electrons are confined along B , p_3 cannot, quantum-mechanically, exceed $\pm \frac{1}{a}$ such the integral becomes simply proportional to $\frac{1}{a}$. This factor completes, inside the integral $\int dk_3$ defining U , the “geometric” $\frac{\sin ak_3}{ak_3}$ evoked above.

k_3 represents the amount of energy-momentum non-conservation of photons along B : this phenomenon cannot indeed but occur at vertices between 3+1-dimensional photons and “confined” electrons (like, as we already mentioned, the non-transversality of $\Pi_{\mu\nu}$). However, the integration dk_3 gets automatically bounded by the rapid decrease of $\frac{\sin ak_3}{ak_3}$ at $|k_3| > \frac{1}{a}$ and this bound is the same as the one for the electron momentum p_3 , $|k_3| \leq \frac{1}{a}$. So, the energy-momentum non-conservation between the outgoing and incoming photons cannot exceed the uncertainty on the electron momentum due to its confinement. In particular, when the graphene strip becomes infinitely thick $a \rightarrow \infty$, this cut-off goes to ∞ and one recovers standard QFT in 3+1 dimensions, with the integration on k_3 going from $-\infty$ to $+\infty$.

4.1 The 1-loop photon propagator in position space

We calculate the 1-loop photon propagator

$$\Delta^{\rho\sigma}(x, y) = \langle 0 | T A^\rho(x) A^\sigma(y) | 0 \rangle \quad (33)$$

and somewhat lighten the notations, omitting symbols like T-product, ...

Introducing the coordinates $u = (u_0, u_1, u_2, u_3)$ and $v = (v_0, v_1, v_2, v_3)$ of the two $(\gamma e^+ e^-)$ vertices one gets at 1-loop

$$\Delta^{\rho\sigma}(x, y) = \int d^4u \int d^4v A^\rho(x) [(ie) A^\mu(u) \bar{\psi}(u) \gamma_\mu \psi(u)] [(ie) A^\nu(v) \bar{\psi}(v) \gamma_\nu \psi(v)] A^\sigma(y). \quad (34)$$

Making the contractions for fermions etc ... yields,

$$\begin{aligned} \Delta^{\rho\sigma}(x, y) = e^2 \int d^4u \int d^4v Tr \int \frac{d^4q}{(2\pi)^4} e^{iq(u-x)} \Delta^{\rho\mu}(q) \gamma_\mu \int \frac{d^4p}{(2\pi)^4} e^{ip(u-v)} G(p) \gamma_\nu \\ \int \frac{d^4r}{(2\pi)^4} e^{ir(v-u)} G(r) \int \frac{d^4s}{(2\pi)^4} e^{is(y-v)} \Delta^{\sigma\nu}(s). \end{aligned} \quad (35)$$

In what follow we shall always omit writing the trace symbol “Tr”.

4.1.1 Standard QFT

One integrates $\int_{-\infty}^{+\infty} d^4u$ and $\int_{-\infty}^{+\infty} d^4v$ for the 4 components of u and v . This gives:

$$\Delta^{\rho\sigma}(x, y) = \int \frac{d^4q}{(2\pi)^4} e^{-iq(x-y)} \Delta^{\rho\mu}(q) \Delta^{\nu\sigma}(q) e^2 \underbrace{\int \frac{d^4p}{(2\pi)^4} \gamma_\mu G(p) \gamma_\nu G(p+q)}_{i\Pi_{\mu\nu}(q)}. \quad (36)$$

When calculating the vacuum polarization the 2 external photon propagators have to be removed, which gives

$$i\Pi_{\mu\nu}(q) = +e^2 \int \frac{d^4p}{(2\pi)^4} \gamma_\mu G(p) \gamma_\nu G(p+q). \quad (37)$$

4.1.2 The case of graphene electrons confined along z

The coordinates u_3 and v_3 of the 2 vertices we do not integrate anymore $\int_{-\infty}^{+\infty}$ but only \int_{-a}^{+a} in which $2a$ is the thickness of the graphene strip. This restriction *localizes the interactions of electrons with photons inside graphene*. So doing, the result that we shall get will only be valid inside graphene, and we shall therefore focus on the “optical properties” of graphene. Indeed, photons also interact with electrons outside graphene but, there, the electron propagators are the ones in the vacuum, not in graphene.

Decomposing $du = d^3\hat{u} du_3$, $dv = d^3\hat{v} dv_3$, we get by standard manipulations

$$\begin{aligned} \Delta^{\rho\sigma}(x, y) = e^2 \int \frac{dp_3}{2\pi} \int \frac{dq_3}{2\pi} \int \frac{dr_3}{2\pi} \int \frac{ds_3}{2\pi} \int_{-a}^{+a} du_3 e^{iu_3(q_3+p_3-r_3)} \int_{-a}^{+a} dv_3 e^{iv_3(-p_3+r_3-s_3)} \\ \int \frac{d^3\hat{q}}{(2\pi)^3} e^{i\hat{q}(\hat{y}-\hat{x})} e^{iq_3(-x_3)} e^{is_3(y_3)} \Delta^{\rho\mu}(\hat{q}, q_3) \Delta^{\sigma\nu}(\hat{q}, s_3) \int \frac{d^3\hat{p}}{(2\pi)^3} \gamma_\mu G(\hat{p}) \gamma_\nu G(\hat{p} + \hat{q}). \end{aligned} \quad (38)$$

Now,

$$\int_{-a}^{+a} dx e^{itx} = 2 \frac{\sin at}{t}, \quad (39)$$

such that

$$\begin{aligned} \Delta^{\rho\sigma}(x, y) = 4 \int \frac{dq_3}{2\pi} \int \frac{ds_3}{2\pi} e^{i(s_3 y_3 - q_3 x_3)} L(a, s_3, q_3) \int \frac{d^3\hat{q}}{(2\pi)^3} e^{i\hat{q}(\hat{y}-\hat{x})} \Delta^{\rho\mu}(\hat{q}, q_3) \Delta^{\sigma\nu}(\hat{q}, s_3) i\Pi_{\mu\nu}(\hat{q}, B), \\ \text{with } L(a, s_3, q_3) = \int_{-\infty}^{+\infty} \frac{dp_3}{2\pi} \frac{dr_3}{2\pi} \frac{\sin a(q_3 + p_3 - r_3)}{q_3 + p_3 - r_3} \frac{\sin a(r_3 - p_3 - s_3)}{r_3 - p_3 - s_3}. \end{aligned} \quad (40)$$

Going from the variables r_3, p_3 to the variables $p_3, h_3 = r_3 - p_3$ one gets

$$L(a, s_3, q_3) = \int_{-\infty}^{+\infty} \frac{dp_3}{2\pi} K(a, s_3, q_3), \quad \text{with } K(a, s_3, q_3) = \int_{-\infty}^{+\infty} \frac{dh_3}{2\pi} \frac{\sin a(q_3 - h_3)}{q_3 - h_3} \frac{\sin a(h_3 - s_3)}{h_3 - s_3}, \quad (41)$$

and the photon propagator at 1-loop writes

$$\begin{aligned} \Delta^{\rho\sigma}(a, x, y) = 4 \int_{-\infty}^{+\infty} \frac{d^3\hat{q}}{(2\pi)^3} e^{i\hat{q}(\hat{y}-\hat{x})} \int_{-\infty}^{+\infty} \frac{ds_3}{2\pi} \int_{-\infty}^{+\infty} \frac{dq_3}{2\pi} e^{i(s_3 y_3 - q_3 x_3)} \Delta^{\rho\mu}(\hat{q}, q_3) K(a, s_3, q_3) \Delta^{\nu\sigma}(\hat{q}, s_3) [\mu] \Pi_{\mu\nu}(\hat{q}, B), \\ \text{with } \mu = \int_{-\infty}^{+\infty} \frac{dp_3}{2\pi}. \end{aligned} \quad (42)$$

Last, going to the variable $k_3 = s_3 - q_3$ (difference of the 3-momentum of incoming and outgoing photon), one gets

$$K(a, s_3, q_3) \equiv \tilde{K}(a, k_3) = \frac{1}{2} \frac{\sin a(s_3 - q_3)}{s_3 - q_3} = \frac{1}{2} \frac{\sin ak_3}{k_3}. \quad (43)$$

After truncating the external photon propagators, one can therefore define an “effective vacuum polarization”

$$\Pi_{\mu\nu}^{eff}(q) = 4\mu \int_{-\infty}^{+\infty} \frac{dk_3}{2\pi} e^{ik_3 y_3} \tilde{K}(a, k_3) (\Delta^{\nu\sigma}(\hat{q}, q_3))^{-1} \Delta^{\nu\sigma}(\hat{q}, q_3 + k_3) \Pi_{\mu\nu}(\hat{q}, B), \quad (44)$$

the meaning of $(\Delta^{\nu\sigma}(\hat{q}, q_3))^{-1}$ being that $\Delta^{\nu\sigma}(\hat{q}, q_3) (\Delta^{\nu\sigma}(\hat{q}, q_3))^{-1} \Delta^{\nu\sigma}(\hat{q}, q_3 + k_3) = \Delta^{\nu\sigma}(\hat{q}, q_3 + k_3)$.

Since we have “localized” electrons inside graphene, we shall conservatively consider

$$p_3 \in \left[-\frac{(\hbar)}{a}, +\frac{(\hbar)}{a}\right] \xleftrightarrow{def} p_3^m = \frac{(\hbar)}{a}, \quad (45)$$

which amounts to take

$$\mu \approx \frac{1}{2\pi} \frac{2(\hbar)}{a} = \frac{(\hbar)}{a\pi}. \quad (46)$$

We work in a system of units where $\hbar = 1$ such that

$$\begin{aligned} \Pi_{\mu\nu}^{eff}(q) &= \frac{1}{\pi^2} \Pi_{\mu\nu}(\hat{q}, B) \times U(q, y_3), \\ U(q, y_3) &= \int_{-\infty}^{+\infty} dk_3 e^{ik_3 y_3} \frac{\sin ak_3}{ak_3} (\Delta^{\nu\sigma}(\hat{q}, q_3))^{-1} \Delta^{\nu\sigma}(\hat{q}, q_3 + k_3), \end{aligned} \quad (47)$$

in which we have used the property that $\Pi_{\mu\nu}(\hat{q}, B)$ can be taken out of the integral. This demonstrates the result that has been announced and introduces the transmittance function $U(q, k_3)$ which is independent of B .

Notice that:

* the 1-loop photon propagator (42) still depends on the difference $\hat{y} - \hat{x}$ but no longer depends on $y_3 - x_3$ only, it is now a function of both y_3 and x_3 (as already mentioned at the end of subsection 2.2, this “extra” dependence is in practice very weak);

* the “standard” calculation corresponds to $\hat{K}(x) = \delta(x) \Rightarrow L(a, s_3, q_3) = \int_{-\infty}^{+\infty} \frac{dp_3}{2\pi} \frac{dr_3}{2\pi} \delta(q_3 + p_3 - r_3) \delta(r_3 - p_3 - s_3) = \int \frac{dp_3}{2\pi} \delta(q_3 - s_3)$. Now, instead, we do not have momentum conservation along z . In particular, while $\hat{q} = \hat{s}$, we do not have the relation $q_3 = s_3$;

* when $a \rightarrow \infty$, there is momentum conservation along B while for finite a it is only approximate.

4.1.3 The transmittance function $U(q, y_3)$. A choice of gauge.

To get our final expression for the transmittance U , we shall hereafter work in the Feynman gauge for the photons in which their propagators are

$$\Delta^{\mu\nu}(q) = -i \frac{g^{\mu\nu}}{q^2}. \quad (48)$$

Then, U can be taken as

$$U(q, y_3) = \int_{-\infty}^{+\infty} dk_3 e^{ik_3 y_3} \frac{\sin ak_3}{ak_3} \frac{q_0^2 - q_1^2 - q_2^2 - q_3^2}{q_0^2 - q_1^2 - q_2^2 - (q_3 + k_3)^2}, \quad (49)$$

in which we recall that the integration variable is $k_3 = s_3 - q_3$, the momentum difference along B between the outgoing and incoming photons.

The analytical properties and pole structure of the integrand in the complex k_3 plane will be seen to play an essential role, like for the transmittance in optics (or electronics). This is why, in addition to its “classical” and “geometric” character, we have given the same name to U .

4.1.4 Going to dimensionless variables

It is time to go to dimensionless variables. We define (p_3^m is given in (45))

$$\eta = a q_0 = \frac{q_0}{p_3^m}, \quad \zeta = a \sqrt{2eB} = \frac{\sqrt{2eB}}{p_3^m}, \quad \Upsilon = \frac{\eta}{\zeta} \gg 1, \quad u = \frac{y_3}{a}. \quad (50)$$

It is also natural, in U , to go to the integration variable $\sigma = \frac{k_3}{p_3^m}$, and to introduce the refractive index n and the angle of incidence θ according to

$$q_2 = 0, \quad q_1 = |\vec{q}| s_\theta = n q_0 s_\theta, \quad q_3 = |\vec{q}| c_\theta = n q_0 c_\theta, \quad \theta \in]0, \frac{\pi}{2}[, \quad (51)$$

which, going to the integration variable $\sigma = a k_3 = \frac{k_3}{p_3^m}$, leads to

$$U(q, y_3) = \frac{1 - n^2}{a} V(u, n, \theta, \eta), \quad V(u, n, \theta, \eta) = \int_{-\infty}^{+\infty} d\sigma e^{i\sigma u} \frac{\sin \sigma}{\sigma} \frac{1}{1 - n^2 - \frac{\sigma}{\eta} (2n \cos \theta + \frac{\sigma}{\eta})}, \quad (52)$$

and, therefore, to

$$\Pi_{\mu\nu}^{eff}(q) = \frac{1}{\pi^2} \Pi_{\mu\nu}(\hat{q}, B) \frac{1-n^2}{a} \times V(u, n, \theta, \eta). \quad (53)$$

We shall also call V the transmittance function.

5 The light-cone equations and their solutions

5.1 Orders of magnitude

In order to determine inside which domains we have to vary the dimensionless parameters, it is useful to know the orders of magnitude of the physical parameters involved in the study.

- The thickness of graphene is $2a \approx 350 \text{ pm} = 350 \cdot 10^{-12} \text{ m}$.
- As we have seen in (45), $|p_3^{max}| \simeq \frac{(\hbar)}{a}$. This gives $(c) p_3^{max} \simeq 1.8 \cdot 10^{-16} \text{ SI}$ or $(c) p_3^{max} \simeq 1.13 \cdot 10^{-6} \text{ GeV} = 1130 \text{ eV} \approx 2.2 \cdot 10^{-3} m_e$.
- To eB corresponds $m^2 = \frac{(\hbar)eB}{(c)^2}$. For example to eB^m (see below) corresponds the mass $\frac{\sqrt{(\hbar)eB^m}}{(c)} \approx 2 \cdot 10^{-33} \text{ kg} \approx 2 \cdot 10^{-3} m_e \ll m_e$.
- $[B] = \frac{[p]^2}{[e](\hbar)}$ such that, to $(p_3^m)^2$ corresponds $B^m \simeq \frac{(\hbar)}{ea^2} \approx 21531 \text{ T}$.
- One has $\zeta \equiv \frac{\sqrt{2e(\hbar)B}}{p_3^m} = \sqrt{2 \frac{B}{B^m}}$. Since $B = \frac{\zeta^2}{2} B^m$, to ζ corresponds the mass $\sqrt{2} \zeta \cdot 10^{-3} m_e$.
- $1 \text{ G} \leftrightarrow \zeta \approx 9.64 \cdot 10^{-5}$, $100 \text{ G} \leftrightarrow \zeta \approx 9.64 \cdot 10^{-4}$, $1 \text{ T} \leftrightarrow \zeta \approx 9.64 \cdot 10^{-3}$, $100 \text{ T} \leftrightarrow \zeta \approx 9.64 \cdot 10^{-2}$.

$$1 \text{ T} \leq B \leq 20 \text{ T} \Leftrightarrow 1/100 \leq \zeta \leq \sqrt{20}/100. \quad (54)$$

- The wavelength of visible light lies between 350 nm and 700 nm , that is between $3.5 \cdot 10^5 \text{ pm}$ and $7 \cdot 10^5 \text{ pm}$. For example light at 500 nm corresponds to an energy $\frac{(hc)}{\lambda} \approx 3.872 \cdot 10^{-19} \text{ SI} \approx 2.48 \text{ eV} \approx (c)p_3^m/200 \ll (c)p_3^{max}$. Likewise, light at 350 nm corresponds to $3.54 \text{ eV} = \frac{6.29}{1000} (c)p_3^m$, and at 800 nm to $1.55 \text{ eV} = \frac{2.75}{1000} (c)p_3^m$.

So, the energy of visible light $\ll (c)p_3^{max}$ and the corresponding η satisfies

$$\text{visible light} \leftrightarrow 2.75 \cdot 10^{-3} \leq \eta \leq 6.3 \cdot 10^{-3}. \quad (55)$$

5.2 The light-cone equations

It is now straightforward to give the expression of the light-cone relations (9) and (10) in the case of graphene. First we express the relevant components of the vacuum polarization $\Pi^{11}, \Pi^{22}, \Pi^{33}$ with dimensionless variables

$$\begin{aligned} \Pi^{11} &= 4\alpha e^{-(n_x^2+n_y^2)\frac{\eta^2}{\zeta^2}} \zeta \eta^2 p_3^m \frac{n_x^2 - n_y^2}{\eta^2 - 4\zeta^2}, \\ \Pi^{22} &= -\hat{\Pi}^{11}, \\ \Pi^{33} &= -4\alpha e^{-(n_x^2+n_y^2)\frac{\eta^2}{\zeta^2}} \zeta p_3^m \frac{\zeta^2 - 2(n_x^2 + n_y^2)\eta^2}{\eta^2 - 4\zeta^2}, \end{aligned} \quad (56)$$

in which $n_x = ns_\theta$ and, since $q_2 = 0$, $n_y = 0$. (53) leads to

$$\begin{aligned} \star \text{ for } A_\perp^\mu : (1-n^2) \left[1 + \frac{p_3^m}{\pi^2} \frac{1}{q_0^2} \Pi^{22}(\alpha, n, \theta, \eta, \zeta) V(u, n, \theta, \eta) \right] &= 0, \\ \star \text{ for } A_\parallel^\mu : (1-n^2) \left[1 + \frac{p_3^m}{\pi^2} \frac{1}{q_0^2} \left(c_\theta^2 \Pi^{11}(\alpha, n, \theta, \eta, \zeta) + s_\theta^2 \Pi^{33}(\alpha, n, \theta, \eta, \zeta) \right) V(u, n, \theta, \eta) \right] &= 0, \end{aligned} \quad (57)$$

and, using (56), to

$$\begin{aligned} \star \text{ for } A_{\perp}^{\mu} : (1 - n^2) \left[1 - \frac{4\alpha}{\pi^2} s_{\theta}^2 n^2 e^{-(ns_{\theta} \frac{\eta}{\zeta})^2} \frac{\zeta}{\eta^2 - 4\zeta^2} V(u, n, \theta, \eta) \right] &= 0, \\ \star \text{ for } A_{\parallel}^{\mu} : (1 - n^2) \left[1 + \frac{\alpha}{\pi^2} s_{\theta}^2 \left(4c_{\theta}^2 n^2 \frac{\zeta}{\eta^2 - 4\zeta^2} + \frac{\zeta}{\eta^2} \frac{8\eta^2 n^2 s_{\theta}^2 - 4\zeta^2}{\eta^2 - 4\zeta^2} \right) e^{-(ns_{\theta} \frac{\eta}{\zeta})^2} V(u, n, \theta, \eta) \right] &= 0. \end{aligned} \quad (58)$$

This defines the index $n = n(\alpha, u, \theta, \eta, \zeta)$.

5.3 Calculating the transmittance V

In order to solve the light cone equations (58), the first step is to compute V , so as to get an algebraic equation for n . V as given by (52) is the Fourier transform of the function $x \mapsto -\eta^2 \frac{\sin x}{x(x-\sigma_1)(x-\sigma_2)}$ where

$$\sigma_1 = -\eta \left(nc_{\theta} - \sqrt{1 - n^2 s_{\theta}^2} \right), \quad \sigma_2 = -\eta \left(nc_{\theta} + \sqrt{1 - n^2 s_{\theta}^2} \right). \quad (59)$$

The Fourier transform of such a product of a cardinal sine with a rational function is well known. The result involves Heavyside functions of the imaginary parts of the poles σ_1, σ_2 , noted Θ_i^+ for $\Theta_i(\Im(\sigma_i))$ and Θ_i^- for $\Theta_i(-\Im(\sigma_i))$.

$$V(u, n, \theta, \eta) = \frac{-\pi\eta^2}{\sigma_1\sigma_2(\sigma_1 - \sigma_2)} \left[(\sigma_1 - \sigma_2) + \sigma_2 \left(\Theta_1^- e^{-i\sigma_1(1-u)} + \Theta_1^+ e^{+i\sigma_1(1+u)} \right) - \sigma_1 \left(\Theta_2^- e^{-i\sigma_2(1-u)} + \Theta_2^+ e^{+i\sigma_2(1+u)} \right) \right]. \quad (60)$$

The poles σ_1, σ_2 are seen to control the behavior of V , thus of n , which depends on the signs of their imaginary parts.

The $\frac{\sin ak_3}{ak_3} \equiv \frac{\sin \sigma}{\sigma}$ occurring in V (see (52)) provides, by its fast decrease, a natural cutoff in k_3 for the integral, $|k_3| \leq \frac{1}{a} = p_3^m$. So, the amount of momentum non-conservation of the photon in the direction of B gets bounded by the inverse of the confinement scale of electrons inside the graphene strip.

The Fourier transform makes the transition between the momentum space in which the propagators of the photons are written, and the position space in which the evolution of the photons is described by the light-cone equations.

It needs to be well defined, which requires in particular that the poles be complex. They are so when $n \notin \mathbb{R}$ or when $ns_{\theta} > 1$, that is when $n_x > 1$.

It cannot be applied when the poles are real, because the integral is no more defined. Then, in particular when $\theta \rightarrow 0$, the integral we shall define as a Cauchy integral, like we did when calculating $\Pi^{\mu\nu}$, arguing in particular of the $+i\varepsilon$ which is understood in the denominator of the outgoing photon propagator. Then, V will be calculated through contour integration in the complex plane.

This alternate method can also be used when the poles are complex. It is comforting that the 2 methods give, at leading order in an expansion at small η and n_2 (n_2 is the imaginary part of the refraction index) the same results. In particular, the cutoff that is then needed to stabilize the integration on the large upper 1/2 circle turns out to be the same as the one that naturally arises in the Fourier transform because of the $\frac{\sin \sigma}{\sigma}$ function.

5.4 Solving the light-cone equations for A_{\parallel}^{μ} and $n \in \mathbb{R} > \frac{1}{\sin \theta}$

That $n \in \mathbb{R}$ largely simplifies the equations.

5.4.1 Calculation of V

Expanding V at leading orders in η , one gets

$$\begin{aligned}\Re(V) &= -\frac{\pi}{\sqrt{n^2 s_\theta^2 - 1}} \eta + \frac{1}{2} \pi (1 + u^2) \eta^2 + \mathcal{O}(\eta^3), \\ \Im(V) &= u n c_\theta \frac{\pi}{\sqrt{n^2 s_\theta^2 - 1}} \eta^2 + \mathcal{O}(\eta^3).\end{aligned}\tag{61}$$

The expansion for $\Im(V)$ in (61) starts at $\mathcal{O}(\eta^2)$ while that of $\Re(V) = \mathcal{O}(\eta)$.

For $n \in \mathbb{R} > \frac{1}{s_\theta}$ the 2 poles σ_1 and σ_2 (59) of V become

$$\sigma_1 = -\eta \left(n \cos \theta - i \sqrt{n^2 s_\theta^2 - 1} \right), \quad \sigma_2 = -\eta \left(n \cos \theta + i \sqrt{n^2 s_\theta^2 - 1} \right); \tag{62}$$

the first term in $\Re(V)$ coincides with $\pm 2i\pi \times$ the residue at the pole σ_1 or σ_2 (the one that lies inside the contour of integration) when one calculates V as a contour integral (see also (66)).

5.4.2 The imaginary parts of the light-cone equations

The imaginary parts of both light-cone equations (58) shrink, for n real, to

$$\Im(V) = 0. \tag{63}$$

It is only rigorously satisfied at $u = 0$, but, (61) and numerical calculations show that, for values of η in the visible spectrum $\eta \in [3/1000, 7/1000]$, $\Im(V) \ll \Re(V) < 1$ and that $\Im(V) \approx 0$ is always an excellent approximation.

5.4.3 There is no non-trivial solution for A_\perp^μ

Detailed numerical investigations show that no solution exists for the transverse polarization but the trivial solution $n = 1$. We shall therefore from now onwards only be concerned with photons A_\parallel^μ with a parallel polarization (see Fig.1).

5.4.4 The light-cone equation for A_\parallel^μ and its solution

Expanding V in powers of η and neglecting $\Im(V)$ enables to get, through standard manipulations, a simple analytical equation for the refraction index n . For $\Upsilon \gg 1$ and $\eta < 7/1000$, the following accurate expression is obtained by expanding (58) in powers of $\frac{1}{\Upsilon}$

$$(1 - n^2) \left[1 - \frac{\alpha}{\pi} \Upsilon \frac{s_\theta^2}{\sqrt{n^2 s_\theta^2 - 1}} \left(1 + \frac{-3n^2 s_\theta^2 - c_\theta^2 + 1/4}{\Upsilon^2} \right) \right] = 0, \tag{64}$$

which leads consistently to the non-trivial solution

$$n^2 \simeq \frac{1}{s_\theta^2} \frac{1 + \left(\frac{\alpha \Upsilon s_\theta^2}{\pi} \right)^2 \left(1 + \frac{1}{2\Upsilon^2} \right)}{1 + 2 \left(\frac{\alpha s_\theta}{\pi} \right)^2 (3s_\theta^2 + c_\theta^2)}, \quad \Upsilon = \frac{\sqrt{2eB}}{q_0}. \tag{65}$$

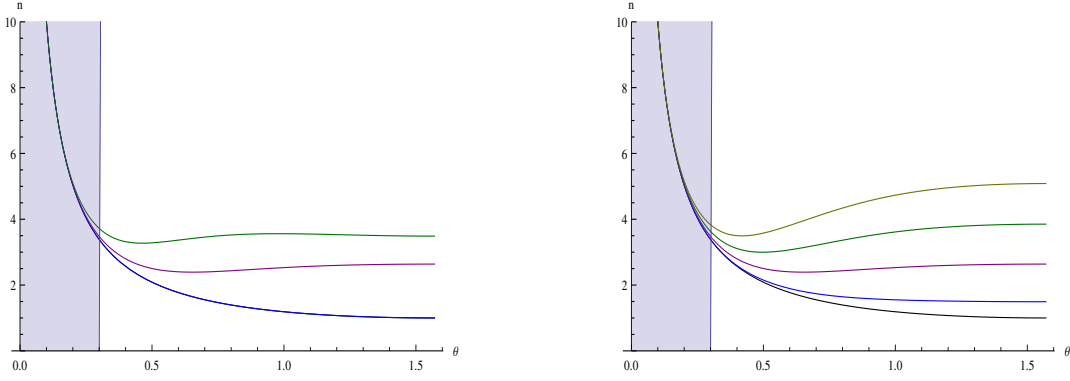


Figure 4: The index $n \in \mathbb{R}$ for A_{\parallel}^{μ} as a function of θ . On the left we vary $\alpha = 1/137$ (blue), 1 (purple), 2 (green) at $\Upsilon = 10$; on the right we vary $\Upsilon = 5$ (blue), 10 (purple), 15 (green), 20 (yellow) at $\alpha = 1$. The lower (black) curves are $1/\sin \theta$

5.4.5 Graphical results and comments

The curves given by our final formula (65) are plotted on Fig.4. On the left we vary α from $\frac{1}{137}$ to 2 at $\Upsilon = \frac{\sqrt{2eB}}{q_0} = 10$ and on the right we keep $\alpha = 1$ and vary Υ between 5 and 20. On both plots, the black lower curve in $n = \frac{1}{\sin \theta}$. We have shaded the domain of low θ in which n must make a transition to another regime (see subsection 5.5).

- The curves go asymptotically to $\frac{1}{s_{\theta}}$ when $\theta \rightarrow 0$. However, we shall see that they should be truncated before $\theta = 0$).
- At large angles, the effects are mainly of quantum nature, strongly influenced by the presence of B and largely depending on the value of α ; when θ gets smaller, one goes to another regime in which the effects of confinement are the dominant ones. The strict limit $\theta \rightarrow 0$ is special (see subsection 5.5).

Quantum 1-loop effects are therefore potentially large at $\alpha \geq 1$. Furthermore, at reasonable values of B and for photons in the visible spectrum, the dependence on B turns out to be strong. The “confinement” of massless Dirac electrons inside a very thin strip of graphene obviously acts as an amplifier of the effects of their interaction with photons in a magnetic background.

- Quantum effects vary inversely to the energy of the photon : low frequencies are favored for testing, and this limit is fortunate since our expansions were done precisely at $\eta = aq_0 \ll 1$.
- For $\eta \ll 1$ and $n > \frac{1}{s_{\theta}}$, the residues of V at the poles σ_1 and σ_2 are

$$res(\sigma_1) = -\frac{\eta}{2i\sqrt{n^2 s_{\theta}^2 - 1}} + \mathcal{O}(\eta^2) = -res(\sigma_2). \quad (66)$$

The agreement between $\Re(V)$ in the first line of (61) and $\pm 2i\pi res(\sigma_1)$ is conspicuous. Indeed, it is easy to prove that for $n \in \mathbb{R}$, only one of the 2 poles lies inside the contour of integration in the upper $1/2$ complex σ -plane which is the alternate method to calculate V .

This confirms that the transmittance function U alone, through its pole(s) is at the origin of the “leading” $\frac{1}{s_{\theta}}$ behavior of the refraction index (see subsection 5.4.6). The poles are nothing more than the ones of the outgoing photon propagator (in the Feynman gauge) $-i\frac{g^{\nu\sigma}}{\bar{q}^2 - (q^3 + k_3)^2}$. We recall that k_3 is the momentum non-conservation along B , which is related (bounded by) to the momentum allowed by quantum mechanics to electrons confined into a strip of thickness $2a$. The non-trivial poles of U (or V) and the leading behavior of the refraction index therefore originate from the sole interactions of photons with “confined” electrons.

- In the approximation that we made, the refractive index does not depend on u , the position inside the strip. This dependence, very weak, only starts to appear through higher orders in the expansion of the transmittance U (or V).

5.4.6 The “leading” $n \sim \frac{1}{s_\theta}$ behavior

It is easy to track the origin of the leading $\frac{1}{s_\theta}$ behavior of the index (we shall see below that the associated divergence at $\theta \rightarrow 0$ is fake).

It comes in the regime when the 2 poles of V lie in different 1/2 planes, such that V can be safely approximated by $V \approx 2i\pi \text{ residue}(\sigma_1 \text{ or } \sigma_2)$.

Keeping only the leading terms in the light-cone equation (58) and using (66) gives then

$$1 - \frac{\alpha}{\pi^2} \frac{\zeta}{\eta^2} \left(2i\pi \frac{\eta}{2i\sqrt{n^2 s_\theta^2 - 1}} \right) = 0, \quad (67)$$

which yields

$$n^2 s_\theta^2 - 1 \sim \left(\frac{\alpha s_\theta^2 \Upsilon}{\pi} \right)^2. \quad (68)$$

The $\frac{1}{s_\theta}$ leading behavior of the index is therefore associated with the transmittance V and is of “geometric” origin (shape of the sample, localization of the interaction vertices inside the graphene strip). This gets confirmed in section 6 where a similar study is done in the absence of any external B : only the $\frac{1}{s_\theta}$ behavior of the index is then practically left over.

5.5 The transition $\theta \rightarrow 0$

It is fairly easy to determine the value of θ below which our calculations and the resulting approximate formula (65) may not be trusted anymore. There presumably starts a transition to another regime.

Our calculations stay valid as long as the 2 poles σ_1 and σ_2 of the transmittance function V lie in different 1/2 planes. This requires that their imaginary parts have opposite signs. Their explicit expressions are given in (86) below. It is then straightforward to get the following condition

$$\sigma_1 \text{ and } \sigma_2 \text{ in different 1/2 planes} \Leftrightarrow n_1^2 > \frac{1 + n_2^2}{\tan^2 \theta}. \quad (69)$$

(69) is always satisfied at $\theta = \frac{\pi}{2}$ and never at $\theta = 0$. Since $n_2 \approx 0$, the transition occurs at

$$n_1(\theta) \approx n(\theta) \approx \frac{1}{\tan \theta}, \quad (70)$$

in which we can use (65) for n . Since at small θ , $\sin \theta \simeq \theta \simeq \tan \theta$, this condition writes approximately

$$1 \leq \frac{1 + \left(\frac{\alpha \Upsilon s_\theta^2}{\pi} \right)^2 \left(1 + \frac{1}{2\Upsilon^2} \right)}{1 + 2 \left(\frac{\alpha s_\theta}{\pi} \right)^2 (3s_\theta^2 + c_\theta^2)} \Leftrightarrow \theta \geq \theta_{\min} = \sqrt{\frac{2}{\Upsilon^2 - \frac{7}{2}}}. \quad (71)$$

For example, at $\Upsilon = 5$ it yields $\theta \geq .3$. Notice that the condition (71) also sets a lower limit $\Upsilon > \sqrt{\frac{7}{2}}$.

It is easy to get the value n_{\max} of n at $\theta = \theta_{\min} \simeq \frac{\sqrt{2}}{\Upsilon}$ given by (71). Plugging this value in (65) one gets

$$n_{\max} \equiv n(\theta = \theta_{\min}) \approx \frac{\Upsilon}{\sqrt{2}}. \quad (72)$$

Seemingly, the solution (65) that we have exhibited gets closer and closer to the “leading” $\frac{1}{s_\theta}$ when θ becomes smaller and smaller. The easiest way to show that this divergent is fake relies on a physical argument: the poles

of the outgoing photon propagator, which are also those of the transmittance U should be such that $|k_3|$, the momentum exchanged with electrons along B is smaller or equal than $\frac{1}{a} = p_3^m$, which is the maximum quantum momentum of the confined electrons of graphene. Mathematically, this traduces for the poles (59) of V by

$$|\sigma_1| \leq 1, \quad |\sigma_2| \leq 1. \quad (73)$$

For $n > \frac{1}{s_\theta}$, both conditions yield ⁹

$$n^2 \leq n_{quant}^2 = \frac{1}{\eta^2} + 1. \quad (74)$$

Remark that n_{max} is much smaller than the quantum limit (74).

The case $\theta = 0$ is special and is investigated directly. One has then $\sigma_1 = -\eta(n-1)$, $\sigma_2 = -\eta(n+1)$, such that $|\sigma_1|, |\sigma_2| \leq 1$, that is

$$n(\theta = 0) \stackrel{quantum}{\leq} \frac{1}{\eta} - 1. \quad (75)$$

For finite η , this bound does not diverge, which shows that the diverging solution (65) cannot be relied on down to $\theta = 0$. It can be trusted at most down to a value of θ for which $n^2 = n_{quant}^2$. Therefore, if a solution exists at $\theta = 0$, n must cross the curve $n = \frac{1}{s_\theta}$ somewhere at small θ .

However, as we now argue, such a transition cannot exist. This is most easily proved by showing that, at no value of θ , $n = \frac{1}{s_\theta}$ can be a solution to the light-cone equation (58). Let us write $\sigma_1 = -\eta \frac{c_\theta}{s_\theta} + \epsilon$, $\sigma_2 = -\eta \frac{c_\theta}{s_\theta} - \epsilon$. The poles being real, V can be calculated by setting $\Theta(0) = \frac{1}{2}$ in (60), which yields

$$\begin{aligned} V \xrightarrow{real \text{ poles}} & -\frac{\pi\eta^2}{\sigma_1\sigma_2(\sigma_1 - \sigma_2)} (\sigma_1 - \sigma_2 + \sigma_2 \cos \sigma_1 e^{i\sigma_1 u} - \sigma_1 \cos \sigma_2 e^{i\sigma_2 u}) \\ = & -\frac{\pi\eta^2}{\sigma_1\sigma_2(\sigma_1 - \sigma_2)} (\sigma_1 - \sigma_2 + \sigma_2 \cos \sigma_1 \cos u \sigma_1 - \sigma_1 \cos \sigma_2 \cos u \sigma_2 + i(\sigma_2 \cos \sigma_1 \sin u \sigma_1 - \sigma_1 \cos \sigma_2 \sin u \sigma_2)). \end{aligned} \quad (76)$$

and, in our case, at $u = 0$,

$$V(u = 0) \approx -\pi \frac{s_\theta^2}{c_\theta^2} \left(1 - \cos(\eta^2 \frac{c_\theta^2}{s_\theta^2}) - \eta \frac{c_\theta}{s_\theta} \sin(\eta \frac{c_\theta}{s_\theta}) \right). \quad (77)$$

The light-cone equation (58) for A_\parallel^μ writes then

$$\left(1 - \frac{1}{s_\theta^2} \right) \left[1 + \frac{\alpha}{\pi} \frac{s_\theta^2}{c_\theta^2} \frac{1}{\zeta} \left(c_\theta^2 - \Upsilon^2 s_\theta^2 (1 - \frac{2}{\Upsilon^2}) \right) \left(1 - \cos(\eta^2 \frac{c_\theta^2}{s_\theta^2}) - \eta \frac{c_\theta}{s_\theta} \sin(\eta \frac{c_\theta}{s_\theta}) \right) \right] = 0, \quad (78)$$

in which we have incorporated the “trivial” term $(1 - n^2)$.

Eq. (78) has no solution: the crossing that would make the connection between our diverging solution and an hypothetical solution in the domain lying below the absolute quantum bound (74) cannot be realized ¹⁰. Hence, the domain in which we can trust our solution (65) cannot be extended down to $\theta = 0$ ¹¹.

Does graphene become “opaque” to photons (total reflection) at very small θ , or is this the sign that, for more and more energetic photons and larger and larger external magnetic fields, the simple model that we made for graphene is no longer valid? We cannot decide in the framework of this limited study. “Something may happen” to photons below a certain angle of incidence, but we must also keep in mind that we only used an expansion of the vacuum polarization dangerously truncated to 1-loop in a situation where $\alpha \simeq 2$.

This investigation will be continued in subsection 5.8.2 for $n \in \mathbb{C}$ (see also the concluding subsection 7.2).

⁹ for $n < \frac{1}{s_\theta}$, the condition $nc_\theta \leq \sqrt{1 - n^2 s_\theta^2}$ must also hold, and then one must have $n^2 \leq 1$ (the case $nc_\theta \geq \sqrt{1 - n^2 s_\theta^2}$ or, equivalently $n^2 \geq 1$ has no solution).

¹⁰We have even investigated the existence of such solutions using the exact expression for V , with the same conclusion. One has to be careful that, in this case, the 2 poles are equal, and the expression of V must therefore be adapted.

¹¹Actually, we have extended our numerical calculations to values of θ for which the 2 poles of V lie in the same $1/2$ plane. They show that, in practice, the solution (65) stays valid even in a small domain below θ_{min} .

5.6 The quantum upper bound $n < n_{quant}$. The threshold at $B = B^m$

We have seen in (74) that Quantum Mechanics sets an upper bound n_{quant} for the index. It is a large value for optical frequencies but, when the energy of photons $q_0 = \frac{\eta}{a}$ increases, n_{quant} decreases accordingly, its asymptotic value being 1 for infinitely energetic photons.

Our calculations being only valid at large $\Upsilon \equiv \frac{\sqrt{2eB}}{q_0} \gg 1$, harder and harder photons need larger and larger values of B (that probably cannot be realized on earth). Then, θ_{min} given in (71) also decreases, while $n_{max} \equiv n(\theta_{min})$ given by (72) increases. A point can be reached at which n_{max} becomes equal, then larger than n_{quant} . $n_{max} \sim n_{quant}$ occurs at $\eta \simeq \frac{\sqrt{2}}{\Upsilon} \Leftrightarrow \zeta \simeq \sqrt{2}$, independently of η . It corresponds (see subsection 5.1) to $B \simeq B^m \approx 21531 T$. B^m appears therefore as the (very large) magnetic field at which the two upper bounds n_{max} and n_{quant} coincide. Still increasing B would result in n_{max} exceeding the quantum limit, which is impossible. So, new phenomena are expected for $B > B^m$, which lie beyond the scope of this work.

5.7 Reliability of the approximation $F(x) \approx \frac{1}{1-x}$ for the electron propagator

The approximation (21) that we made for the expression of the electron propagator inside graphene (see subsection 3.1.2) is only valid for low energy electrons with $p_0 \leq 1.2\sqrt{2eB}$. Using subsection 5.1 for the orders of magnitude, the lowest external magnetic field $B = 1 T$ that we consider corresponds to $\zeta \approx \frac{1}{100}$ and therefore to an energy $\approx \sqrt{2} \frac{1}{100} 10^{-3} m_e \approx 7 eV$. Accordingly, our approximation is reliable for electrons with energy $p_0 \leq 10 eV$. This is satisfied inside graphene.

Note that the visible light that we send through graphene has also energy $\leq 3.5 eV$.

5.8 Going to $n \in \mathbb{C}$

5.8.1 The case of A_{\parallel}^{μ}

Numerical calculations can be performed in the general case of a complex index $n = n_1 + in_2$. They show in particular that $|n_2| \ll n_1$, confirming the reliability of the approximation that we made in the main stream of this study (we have limited them to values of θ large enough for our equations to be valid). The results are displayed on Fig.5, in which we plot n_2 as a function of θ , varying α (left) and Υ (right), and on Fig.6 in which we plot n_2 as a function of u , varying Υ .

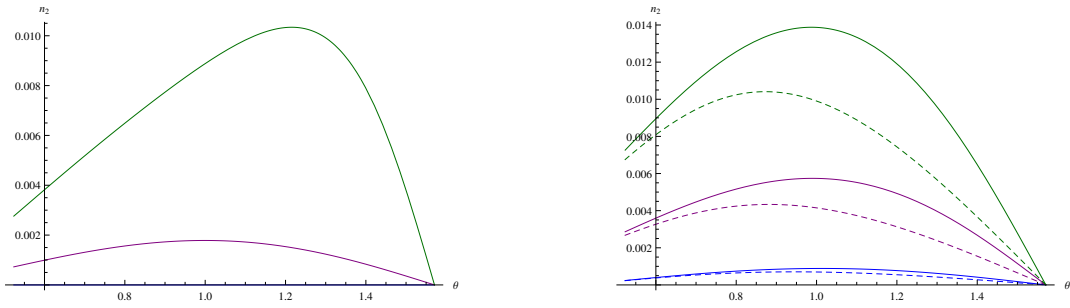


Figure 5: The imaginary part n_2 of the index n for A_{\parallel}^{μ} as a function of θ . On the left we vary $\alpha = 1/137$ (blue), 1 (purple), 2 (green) at $\Upsilon = 5$; on the right we vary $\Upsilon = 4$ (blue), 8 (purple), 12 (green) at $\alpha = 1$. The dashed curves on the right correspond to the rough approximation (81)

To this purpose, and because the real part of the light-cone equation only gets very slightly modified, it is enough to consider the imaginary part of the light-cone equation (58) for A_{\parallel}^{μ} in which we plug, for n_1^2 , the analytic expression

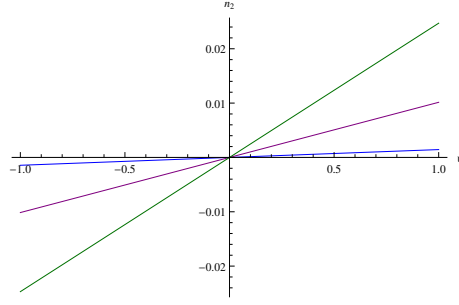


Figure 6: The imaginary part n_2 of index n for A_{\parallel}^{μ} as a function of u . We take $\alpha = 1$, $\eta = 5/1000$, and vary $\Upsilon = 4$ (blue), 8 (purple), 12 (green)

(65). In practice, the expansion of this equation at $\mathcal{O}(\eta^2)$ and $\mathcal{O}(n_2)$, which is a polynomial of first order in n_2 is enough for our purposes. An important ingredient of the calculation is the expansion of the transmittance V at order $\mathcal{O}(\eta^2)$ and $\mathcal{O}(n_2)$, in the case when its 2 poles lie in different $1/2$ planes, which writes

$$\begin{aligned} \frac{1}{\pi} \Re(V) &= -\frac{\eta}{\sqrt{n_1^2 s_{\theta}^2 - 1}} + \frac{1}{2}(1 + u^2)\eta^2 + \frac{uc_{\theta}(2n_1^2 s_{\theta}^2 - 1)}{(n_1^2 s_{\theta}^2 - 1)^{\frac{3}{2}}}\eta^2 n_2 + \dots, \\ \frac{1}{\pi} \Im(V) &= \frac{un_1 c_{\theta}}{\sqrt{n_1^2 s_{\theta}^2 - 1}}\eta^2 - \frac{n_1 s_{\theta}^2}{(n_1^2 s_{\theta}^2 - 1)^{\frac{3}{2}}}\eta n_2 + \dots \end{aligned} \quad (79)$$

The corresponding analytical expression for n_2 , an odd function of u , is long and unaesthetic and we only give it in footnote 12¹². However a rough order of magnitude can be obtained with very drastic approximations which lead to the equation

$$n_2 s_{\theta}^2 \sim u \eta c_{\theta} (n_1^2 s_{\theta}^2 - 1), \quad (81)$$

in which, like before, we can plug in the analytical formula (65) for n_1^2 . The corresponding curves are the dashed ones in Fig.5¹³.

As B increases, it is no longer a reliable approximation to consider the index to be real : absorption becomes non-negligible. The window of medium-strong B 's from 1 to 20 Teslas together with photons in the visible range appears therefore quite simple and special. Outside this window, the physics is most probably much more involved and equations much harder to solve.

5.8.2 The “wall” for A_{\parallel}^{μ}

The situation is best described in the complex (n_1, n_2) plane of the solutions $n = n_1 + in_2$ of the light-cone equation (58) for A_{\parallel}^{μ} , which decomposes into its real and imaginary parts (in the limit $\eta \ll \zeta \Leftrightarrow \Upsilon \gg 1$, and neglecting the exponential $e^{-\frac{n_2^2 s_{\theta}^2}{\Upsilon^2}}$ which plays a negligible role) according to

$$\begin{aligned} * \quad & 1 + \frac{\alpha}{\pi} \frac{s_{\theta}^2}{\zeta} \left(1 + \frac{1}{4\Upsilon^2} \right) [(\Upsilon^2 - (n_1^2 - n_2^2)(1 + s_{\theta}^2)) \Re(V) + 2n_1 n_2 (1 + s_{\theta}^2) \Im(V)] = 0, \\ * \quad & -2n_1 n_2 (1 + s_{\theta}^2) \Re(V) + (\Upsilon^2 - (n_1^2 - n_2^2)(1 + s_{\theta}^2)) \Im(V) = 0. \end{aligned} \quad (82)$$

¹²The imaginary part of the light-cone equation for A_{\parallel}^{μ} writes

$$\begin{aligned} M + N n_2 &= 0, \\ M &= u \zeta c_{\theta} s_{\theta}^2 (-1 + n_1^2 s_{\theta}^2) + \frac{1}{4\zeta} \eta^2 u c_{\theta} s_{\theta}^2 (1 - 4n_1^2 c_{\theta}^2 - 12n_1^2 s_{\theta}^2) (-1 + n_1^2 s_{\theta}^2), \\ N &= -\frac{\zeta s_{\theta}^4}{\eta} - \frac{1}{\zeta} \eta^2 (1 + u^2) s_{\theta}^2 (c_{\theta}^2 + 3s_{\theta}^2) (-1 + n_1^2 s_{\theta}^2)^{\frac{3}{2}} + \frac{1}{4\zeta} (-8\eta c_{\theta}^2 s_{\theta}^2 - 25\eta s_{\theta}^4 + 12\eta n_1^2 c_{\theta}^2 s_{\theta}^4 + 36\eta n_1^2 s_{\theta}^6). \end{aligned} \quad (80)$$

¹³The agreement with the exact curves worsens as α increases.

All previous calculations favoring solutions with low absorption $|n_2| \ll n_1$, it is in this regime that we shall investigate the presence of a “wall” at small θ . To this purpose, we shall plug into the light-cone equation (58) for A_{\parallel}^{μ} the expansion of the transmittance V that is written in (79).

The situation at $\theta = \frac{\pi}{4}$ (left) and $\theta = \frac{\pi}{10}$ are depicted in Fig.7. The values of the parameters are $\alpha = 1, u = .5, \eta = \frac{5}{1000}, \Upsilon = 5$.

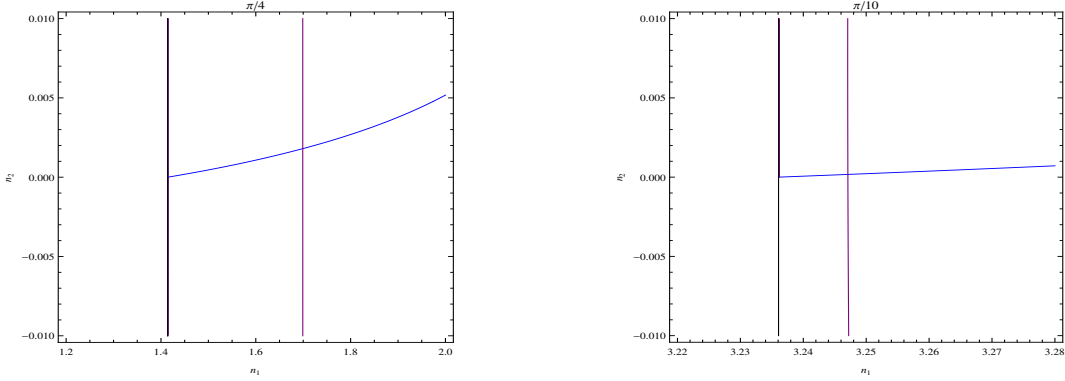


Figure 7: The index (n_1, n_2) for A_{\parallel}^{μ} at $\theta = \frac{\pi}{4}$ (left) and $\theta = \frac{\pi}{10}$ (right)

The purple curve corresponds to the solutions of the real part of the light-cone equation and the blue quasi-vertical line to the solution of its real part. The intersection of the 2 curves yields the solution $n = n_1 + in_2$. We recover $|n_2| \ll n_1$. The black vertical line on the left corresponds to $n_1 = \frac{1}{s_{\theta}}$.

A transition brutally occurs close to $\theta = \frac{\pi}{14}$. Then the solution at $|n_2| \ll n_1 = \mathcal{O}(1)$ disappears. It is clearly visible on Fig.8 below in which we plot the situation after the transition, for $\theta = \frac{\pi}{17}$.

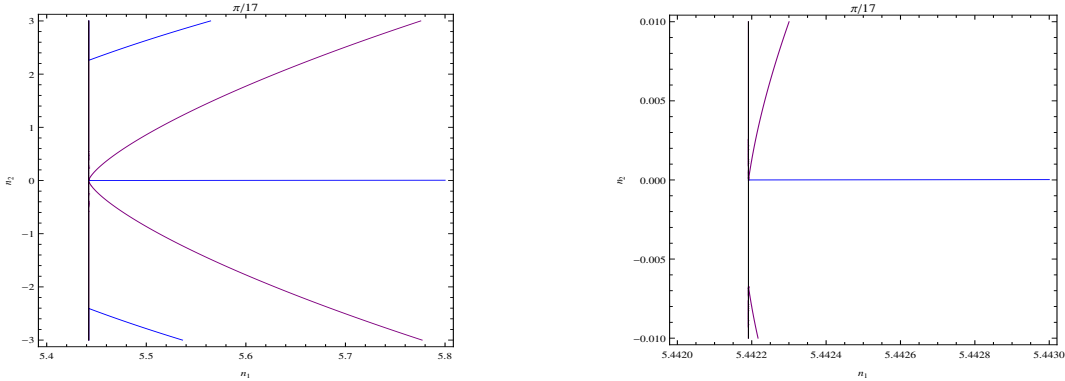


Figure 8: The index (n_1, n_2) for A_{\parallel}^{μ} at $\theta = \frac{\pi}{17}$. The right figure is an enlargement of the left one

There is no more intersection between the solutions of the real (purple) and imaginary (blue) parts of the light-cone equations, except at $n_2 = 0, n_1 = \frac{1}{s_{\theta}}$, which is a fake solution since we know that n_1 can never reach its “asymptotic” value $\frac{1}{s_{\theta}}$.

5.8.3 An estimate of the angle of transition θ_{min}

This change of regime is characterized by a brutal jump in the value of n_2 , which should be manifest on the imaginary part of the light-cone equation (82). A very reliable approximation can be obtained by truncating $\Re(V)$

to its first term, in which case one gets

$$n_2 \approx (n_1^2 s_\theta^2 - 1) \frac{u\eta c_\theta (\Upsilon^2 - n_1^2(1 + s_\theta^2))}{s_\theta^2 (\Upsilon^2 - n_1^2(1 + s_\theta^2)) - 2(1 + s_\theta^2)(n_1^2 s_\theta^2 - 1)} \quad (83)$$

which has a pole at (we use $s_\theta^2 \ll 1$)

$$n_1^2 \approx \frac{2 + \Upsilon^2 s_\theta^2}{3s_\theta^2}. \quad (84)$$

This value for n_1 determines the maximum that can be reached when θ decreases. Indeed, then, n_2 becomes out of control in the framework of our approximations. We also know that n_1 should stay below $\frac{1}{s_\theta}$. The intersection of (84) and $\frac{1}{s_\theta}$ yields the lower limit for θ

$$\theta_{min} \sim \frac{1}{\Upsilon}. \quad (85)$$

(85) is smaller than our previous estimate (71) obtained in the approximation $n \in \mathbb{R}$.

At $\Upsilon = 5$ one gets $\theta_{min} \approx \frac{\pi}{15}$, which shows the reliability of our estimate (the true transition numerically occurs between $\frac{\pi}{14}$ and $\frac{\pi}{15}$).

5.8.4 The case of A_\perp^μ

We only summarize below the steps that lead to the conclusion that no solution to the refraction index except the trivial $n = 1$ exists for the transverse polarization.

Starting from the corresponding light-cone equation in (58), the main task is to get the appropriate expression for the transmittance function V . To this purpose the starting point is the general expression (60). We expand it in powers of η in the sense that the exponentials are expanded at $\mathcal{O}(\eta)$ or, eventually $\mathcal{O}(\eta^2)$. No expansion in powers of n_2 is done because, if solutions exist, they may occur for fairly large values of n_2 (and n_1).

Since the sign of the imaginary parts of the poles σ_1 and σ_2 obviously play a central role, it is also useful to extract

$$\begin{aligned} \Im(\sigma_1) &= \eta \left(-n_2 c_\theta + \frac{1}{\sqrt{2}} \sqrt{-c + \sqrt{c^2 + d^2}} \right), \\ \Im(\sigma_2) &= \eta \left(-n_2 c_\theta - \frac{1}{\sqrt{2}} \sqrt{-c + \sqrt{c^2 + d^2}} \right), \\ c &= 1 - (n_1^2 - n_2^2) s_\theta^2, \quad d = 2n_1 n_2 s_\theta^2. \end{aligned} \quad (86)$$

Straightforward manipulations on (60) show that:

- * when $n_2 > 0$ ($\Rightarrow \Im(\sigma_2) < 0$): if $\Im(\sigma_1) > 0$, $V = \frac{-i\pi\eta}{\sqrt{1-n^2s_\theta^2}} + \dots$; if $\Im(\sigma_1) < 0$, $V = \frac{\pi\eta^2}{2}(1-u)^2 + \dots$
- * when $n_2 < 0$ ($\Rightarrow \Im(\sigma_1) > 0$): if $\Im(\sigma_2) > 0$, $V = \frac{\pi\eta^2}{2}(1+u)^2 + \dots$; if $\Im(\sigma_2) < 0$, $V = \frac{-i\pi\eta}{\sqrt{1-n^2s_\theta^2}} + \dots$

The cases when $V = \mathcal{O}(\eta^2)$ correspond to σ_1 and σ_2 being in the same $1/2$ complex σ -plane.

When $V = \frac{-i\pi\eta}{\sqrt{1-n^2s_\theta^2}}$, its real and imaginary parts are given by

$$\Re(V) = \frac{\pi\eta n_1 n_2 s_\theta^2}{\sqrt{2}} \frac{\sqrt{c + \sqrt{c^2 + d^2}}}{\sqrt{c^2 + d^2}}, \quad \Im(V) = \frac{-\pi\eta}{\sqrt{2}} \frac{\sqrt{-c + \sqrt{c^2 + d^2}}}{\sqrt{c^2 + d^2}}. \quad (87)$$

Numerical solutions of the light-cone equation show that no solution exists that fulfill the appropriate criteria on the signs of $\Im(\sigma_1)$, $\Im(\sigma_2)$. For example, for $n_2 < 0$, one gets solutions shared by both the real and imaginary parts of the light-cone equations, but they satisfy $\Im(\sigma_2) > 0$ and must therefore be rejected.

The next step is to use the exact expression (60) of V , but no acceptable solution exists (solutions with very large values of n_1 and n_2 , larger than 20, are a priori rejected).

6 The case $B = 0$

6.1 The vacuum polarization $\Pi^{\mu\nu}$

Standard techniques applied to massless electrons of graphene at the Dirac point lead to the exact results

$$\begin{aligned}
i\Pi_{\cancel{X}}^{11}(\hat{q}) &= i\frac{e^2}{8} \left(\sqrt{\hat{q}_E^2} - \frac{q_1^2}{\sqrt{\hat{q}_E^2}} \right), \\
i\Pi_{\cancel{X}}^{22}(\hat{q}) &= i\frac{e^2}{8} \left(\sqrt{\hat{q}_E^2} - \frac{q_2^2}{\sqrt{\hat{q}_E^2}} \right), \\
i\Pi_{\cancel{X}}^{33} &= i\frac{e^2}{4} \sqrt{\hat{q}_E^2}, \\
i\Pi_{\cancel{X}}^{00} &= -i\frac{e^2}{8} \frac{q_1^2 + q_2^2}{\sqrt{\hat{q}_E^2}}, \\
i\Pi_{\cancel{X}}^{12} &= -i\frac{e^2}{8} \frac{q_1 q_2}{\sqrt{\hat{q}_E^2}}, \\
i\Pi_{\cancel{X}}^{01} &= -\frac{e^2}{8} \frac{q_0^E q_1}{\sqrt{\hat{q}_E^2}}, \\
i\Pi_{\cancel{X}}^{02} &= -\frac{e^2}{8} \frac{q_0^E q_2}{\sqrt{\hat{q}_E^2}}, \\
\Pi_{\cancel{X}}^{03} &= \Pi_{\cancel{X}}^{13} = \Pi_{\cancel{X}}^{23} = 0.
\end{aligned} \tag{88}$$

in which $q_0 = iq_0^E$ and $(\hat{q}^E)^2 = (q_0^E)^2 + q_1^2 + q_2^2$.

★ $\Pi_{\cancel{X}}^{ij}$ is proportional to $\pi\alpha$ while, in the presence of B , it was proportional to α . The extra π comes from $\int_0^1 dx \sqrt{x(1-x)} = \frac{\pi}{8}$.

★ Transversality: one easily checks on (88) that $q_0\Pi_{\cancel{X}}^{00} + q_1\Pi_{\cancel{X}}^{10} + q_2\Pi_{\cancel{X}}^{20} = 0$, $q_0\Pi_{\cancel{X}}^{01} + q_1\Pi_{\cancel{X}}^{11} + q_2\Pi_{\cancel{X}}^{21} = 0$, $q_0\Pi_{\cancel{X}}^{02} + q_1\Pi_{\cancel{X}}^{12} + q_2\Pi_{\cancel{X}}^{22} = 0$. The last condition $q_0\Pi_{\cancel{X}}^{03} + q_1\Pi_{\cancel{X}}^{13} + q_2\Pi_{\cancel{X}}^{23} + q_3\Pi_{\cancel{X}}^{33} = 0$ reduces to $q_3\Pi_{\cancel{X}}^{33} = 0$, which is not satisfied unless $q_3 = 0$ or $\hat{q}_E^2 = 0$ (“on mass shell 2+1 photon”).

In our setup, we recall $n^2 = \frac{q_1^2 + q_2^2 + q_3^2}{q_0^2}$, $n_x = \frac{q_1}{q_0} = ns_\theta$, $n_z = \frac{q_3}{q_0} = nc_\theta$. One has $(\hat{q}_E)^2 = (q_0^E)^2 + q_1^2 + q_2^2 = q_0^2(n^2 s_\theta^2 - 1)$ because $q_3 = 0$. So, $\sqrt{\hat{q}_E^2} = \pm q_0 \sqrt{n^2 s_\theta^2 - 1}$. This gives

$$\begin{aligned}
\Pi_{\cancel{X}}^{11} &= \mp \frac{\pi\alpha}{2} q_0 \frac{1}{\sqrt{n^2 s_\theta^2 - 1}}, \\
\Pi_{\cancel{X}}^{22} &= \pm \frac{\pi\alpha}{2} q_0 \sqrt{n^2 s_\theta^2 - 1}, \\
\Pi_{\cancel{X}}^{33} &= \pm \pi\alpha q_0 \sqrt{n^2 s_\theta^2 - 1}, \\
\Pi_{\cancel{X}}^{00} &= \mp \frac{\pi\alpha}{2} q_0 \frac{n^2 s_\theta^2}{\sqrt{n^2 s_\theta^2 - 1}}, \\
\Pi_{\cancel{X}}^{12} &= 0, \quad \Pi_{\cancel{X}}^{i3} = 0, \\
\Pi_{\cancel{X}}^{01} &= \pm \frac{\pi\alpha}{2} q_1 \frac{1}{\sqrt{n^2 s_\theta^2 - 1}}, \\
\Pi_{\cancel{X}}^{02} &= \pm \frac{\pi\alpha}{2} q_2 \frac{1}{\sqrt{n^2 s_\theta^2 - 1}}.
\end{aligned} \tag{89}$$

6.2 The light-cone equation and the refractive index

The light-cone equations (57) together with (89) yield

$$\begin{aligned} \text{for } A_{\perp}^{\mu} : (1 - n^2) \left[1 \pm \frac{\alpha}{\eta} \sqrt{n^2 s_{\theta}^2 - 1} \frac{V(u, \rho, n, \theta, \eta)}{\pi} \right] &= 0, \\ \text{for } A_{\parallel}^{\mu} : (1 - n^2) \left[1 \pm \frac{\alpha}{\eta} \left(-\frac{c_{\theta}^2}{2\sqrt{n^2 s_{\theta}^2 - 1}} + s_{\theta}^2 \sqrt{n^2 s_{\theta}^2 - 1} \right) \frac{V(u, \rho, n, \theta, \eta)}{\pi} \right] &= 0. \end{aligned} \quad (90)$$

in which V is the same transmittance function as before, given by (52).

6.3 Solutions for A_{\parallel}^{μ} with $n \in \mathbb{R}$

We approximate, at $\eta \ll 1$, according to (61), $V \approx -\frac{\eta\pi}{\sqrt{n^2 s_{\theta}^2 - 1}}$.

Like in the presence of B , no non-trivial solution exists for the transverse polarization and we focus hereafter on A_{\parallel}^{μ} . The corresponding light-cone equation writes

$$1 \pm \alpha \left(-\frac{c_{\theta}^2}{2(n^2 s_{\theta}^2 - 1)} + s_{\theta}^2 \right) = 0, \quad (91)$$

(91) has seemingly 2 types of solutions, the first with $n > \frac{1}{s_{\theta}}$ and the second with $n < \frac{1}{s_{\theta}}$. They write respectively

$$\begin{aligned} * \ n > \frac{1}{s_{\theta}} : n^2 &= \frac{1}{s_{\theta}^2} \left(1 + \frac{\alpha c_{\theta}^2}{2(1 + \alpha s_{\theta}^2)} \right), \\ * \ n < \frac{1}{s_{\theta}} : n^2 &= \frac{1}{s_{\theta}^2} \left(1 - \frac{\alpha c_{\theta}^2}{2(1 - \alpha s_{\theta}^2)} \right). \end{aligned} \quad (92)$$

They are plotted on Fig.9, respectively on the left for $n > \frac{1}{s_{\theta}}$ and on the right for $n < \frac{1}{s_{\theta}}$. They only depend on α and we plot them for $\alpha = \frac{1}{137}$ (blue), $\alpha = 1$ (purple) and $\alpha = 1.5$ (green), $\alpha = 2$ (yellow) together with $n = \frac{1}{s_{\theta}}$ (black), the latter being in practice indistinguishable from $\alpha = \frac{1}{137}$.

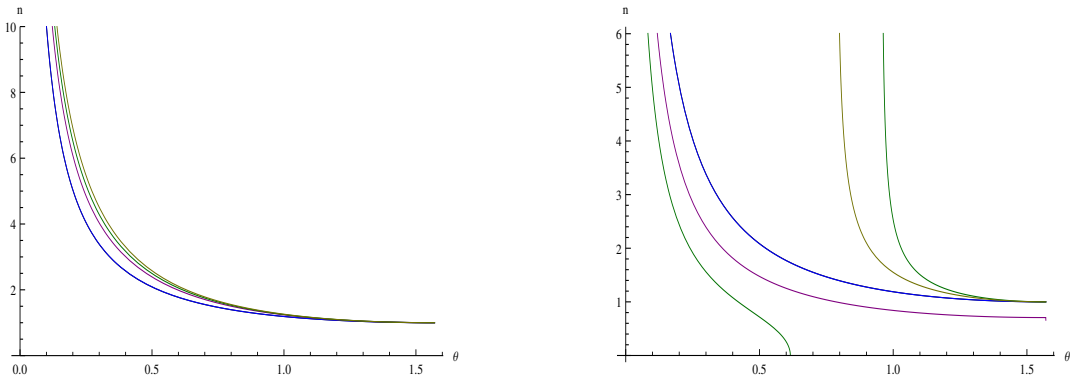


Figure 9: The 2 types of real solutions of the light-cone equation for A_{\parallel}^{μ} as a function of θ when no external B is present. On the left $n > \frac{1}{s_{\theta}}$, on the right $n < \frac{1}{s_{\theta}}$. We vary $\alpha = 1/137$ (blue), 1 (purple), 1.5 (green), 2 (yellow). The black (\simeq blue) curves are $1/\sin \theta$

Looking at the curves, it is conspicuous that one cannot trust them, neither when $\theta \rightarrow 0$ because of divergences, nor when θ becomes large for $\alpha > 1$. In particular, the solution with $n < \frac{1}{s_{\theta}}$ becomes out of control above $\theta \geq .5$; it furthermore cannot exist when $s_{\theta}^2 > \frac{1}{\alpha}$ since then $n > \frac{1}{s_{\theta}}$ (a divergence occurs at $s_{\theta}^2 = \frac{1}{\alpha}$).

The approximation of considering $n \in \mathbb{R}$ is obviously very hazardous, specially when $\alpha > 1$. This is why we shall perform in subsection 6.4 a detailed study with $n \in \mathbb{C}$.

6.4 Solutions with $n \in \mathbb{C}$

6.4.1 There is no solution with $n_1 < \frac{1}{s_\theta}$

When supposing $n \in \mathbb{R}$, we have seen that the solution with $n < \frac{1}{s_\theta}$ was unstable, in particular above θ_{max} such that $(\sin \theta_{max})^2 = \frac{1}{\alpha}$ were it did not exist anymore.

Careful investigations for $n \in \mathbb{C}$ show that, like in the presence of B , no solution with $n_1 < \frac{1}{s_\theta}$ exists¹⁴.

6.4.2 The solution with $n_1 > \frac{1}{s_\theta}$

In the presence of an external B , we have seen that the solution with a quasi-real index suddenly disappears below an angle $\theta_{min} \approx \frac{1}{\Upsilon}$. In the present case with no external B , there is no θ_{min} but the index becomes “more and more complex” (that is the ratio of its imaginary and real parts increase) when θ becomes smaller and smaller.

To demonstrate this, we study the light-cone equation (90) for A_{\parallel}^{μ} with $n = n_1 + in_2$, $n_1, n_2 \in \mathbb{R}$. For practical reasons, we shall limit ourselves to the expansion of V at small η and n_2 , valid when the 2 poles of V lie in different 1/2 planes, given in (79).

The results are displayed in Fig.10 below, for $\alpha = 1$ (blue), $\alpha = 1.5$ (purple) and $\alpha = 2$ (green). The values of n_1 are plotted on the left and the ones of n_2 on the right. The value of the other parameters are $u = .5$, $\eta = \frac{5}{1000}$. For $\alpha = \frac{1}{137}$, n_1 is indistinguishable from $\frac{1}{s_\theta}$.

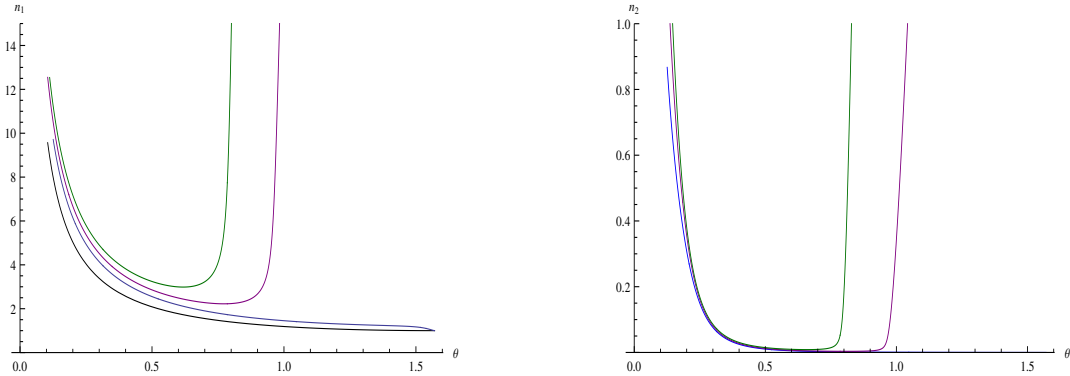


Figure 10: The real part n_1 (left) and imaginary part n_2 (right) of the solution n of the light-cone equation (90) for A_{\parallel}^{μ} in the absence of external B . The blue curves correspond to $\alpha = 1$, the purple curves to $\alpha = 1.5$ and the green curves to $\alpha = 2$. The black curve on the left is $n_1 = \frac{1}{s_\theta}$.

- As θ gets smaller and smaller, the index becomes complex with larger and larger values of both its components. It is of course bounded as before to $|n| < \frac{1}{\eta}$ by quantum considerations. The brutal transition at $\theta_{min} \simeq \frac{1}{\Upsilon}$ is replaced by a smooth transition (which could be anticipated since, in the absence of B , the parameter Υ does not exist).

¹⁴In this case, the expansion of the transmittance V at small η and n_2 writes

$$\begin{aligned} \frac{1}{\pi} \Re(V) &= \frac{un_1 c_\theta}{\sqrt{1 - n_1^2 s_\theta^2}} \eta^2 + \frac{1}{2} (1 + u^2) \eta^2 - \frac{n_1 s_\theta^2}{(1 - n_2^2 s_\theta^2)^{\frac{3}{2}}} \eta n_2 + \dots \\ \frac{1}{\pi} \Im(V) &= -\frac{\eta}{\sqrt{1 - n_1^2 s_\theta^2}} + \frac{uc_\theta (2n_1^2 s_\theta^2 - 1)}{(1 - n_2^2 s_\theta^2)^{\frac{3}{2}}} \eta^2 n_2 + \dots \end{aligned} \quad (93)$$

that we plug into the light-cone equation (90) for A_{\parallel}^{μ} .

- A new feature seems to occur, the presence of a “wall” at large θ for $\alpha > 1$, obviously reminiscent of the divergence that occurred in the approximation $n \in \mathbb{R}$ at $\theta = \theta_{max}$, $(\sin \theta_{max})^2 = \frac{1}{\alpha}$ for the solution $n < \frac{1}{s_\theta}$ (we had noticed that this condition could no longer be satisfied since, for $s_\theta^2 > \frac{1}{\alpha}$, n could only be larger than $\frac{1}{s_\theta}$).

Three explanations come to the mind concerning this wall. The first is that, for large values of n_2 , the expansion (79) that we used for V is no longer valid; however, using the exact expression for the transmittance leads to the same conclusion. The second, and also very likely one, is that the perturbative series has no meaning whatsoever for $\alpha > 1$ (2-loop corrections become larger than 1-loop etc); using a 2-loop calculation of the vacuum polarization without external B seems feasible but also goes beyond the scope of this work. The third is that this divergence is the sign that some physical phenomenon occurs, like total reflexion, for $\theta > \theta_{max}$, which can only be settled by experiment.

- These calculations show in which domain the approximation $n \in \mathbb{R}$ is reliable since it requires $n_2 \ll 1$: for example $n_2 < .1$ needs $.3 \leq \theta \leq \theta_{max}$, which leaves (except for $\alpha \leq 1$ in which case $\theta_{max} \geq \frac{\pi}{2}$) only a small domain for θ .

• A very weak dependence on α for $\theta < \theta_{max}$

In the absence of external B and away from the “wall” at large θ , the index is seen to depend very little on α . The dependence of n on θ is practically only due to the transmittance function V and to the confinement of electrons inside graphene. Notice in particular that, when $\alpha = \frac{1}{137} \ll 1$, the curve is indistinguishable from that of $\frac{1}{s_\theta}$.

The fairly large dependence on α that we uncovered in the presence of B are therefore triggered by B itself.

- **The dependence on the energy of the photon** The dependence on η only occurs in the imaginary part n_2 of n . This is shown in Fig.11, in which we vary η in the visible spectrum, $\eta \in [\frac{2}{1000}, \frac{7}{1000}]$ at $\alpha = 1.5$ (unlike in Fig.10, θ has not been extended above θ_{max}).

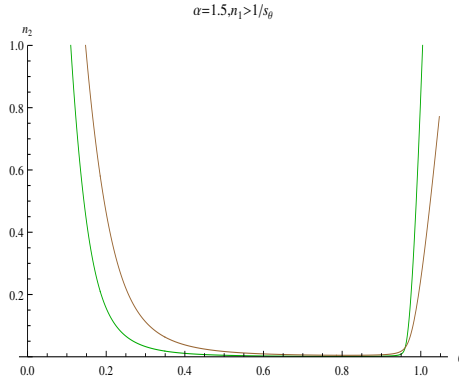


Figure 11: n_2 as a function of θ for $\eta = \frac{2}{1000}$ (green) and $\eta = \frac{7}{1000}$ (brown), in the case $\alpha = 1.5$

6.5 The limit of very small θ ; absorption of visible light and experimental opacity

6.5.1 At small θ

Since absorption of visible light by graphene at close to normal incidence has been measured [11], let us show that our simple model gives predictions that are compatible with these measurements.

To that purpose, we calculated numerically the index n at the lowest value of θ at which the 2 poles of V lie in different $1/2$ planes. We have used the exact expression of V (no expansion) and obtained

$$\begin{aligned} * \text{ for } \alpha = 1 \text{ and } \theta = \frac{\pi}{105.9} : n = 41.20 + .7 \times i, \\ * \text{ for } \alpha = 2 \text{ and } \theta = \frac{\pi}{89} : n = 40 + 1 \times i. \end{aligned} \quad (94)$$

The 2 corresponding angles are small enough to be considered close to normal incidence.

The transmission coefficient along z (therefore for $c_\theta \approx 1$) is given by

$$T = e^{-8\pi\eta n_2 c_\theta} \approx 1 - 8\pi\eta n_2, \quad (95)$$

while experimental measurements [11] are compatible with

$$T \approx 1 - \pi \alpha_{vac}, \quad \alpha_{vac} = \frac{1}{137}. \quad (96)$$

This requires

$$n_2 \approx \frac{\alpha_{vac}}{8\eta} \in [.46, .13] \text{ for } \eta \in \left[\frac{2}{1000}, \frac{7}{1000} \right]. \quad (97)$$

We get therefore the correct order of magnitude for n_2 . The discrepancy between our prediction and the experimental value can be thought as an estimate of 2-loop corrections in the absence of B .

6.5.2 At $\theta = 0$

At $\theta = 0$, \vec{q} is parallel to the z axis such that there is no more distinction between transverse and parallel polarizations. Since we have found for $\theta \neq 0$ no non-trivial solution to the light-cone equation for A_\perp^μ , but only the trivial one $n = 1$, a smooth limit at $\theta = 0$, which should be common for the 2 polarizations, would presumably require that, like for A_\perp^μ , only $n = 1$ remains for A_\parallel^μ , too; but we have yet no proof of this.

So, like in the presence of B , we are at a loss to give any prediction at $\theta = 0$. This is for sure a limitation of our model.

7 Outlook and prospects

7.1 General remarks

We have shown that the refractive index of graphene in the presence of an external magnetic field is very sensitive to 1-loop quantum corrections. The effects are large for optical wavelengths and even for magnetic fields below 20 Teslas. They only depend (at least for the real part of the refractive index), on the ration $\frac{\sqrt{2eB}}{q_0}$ which makes them larger and larger as the photon goes to smaller and smaller energy. We only found them for so-called parallel polarization of the photon. At the opposite, when there is no external B , quantum effects stay small and the optical properties of graphene are mainly controlled by the sole transmittance function which incorporates the geometry of the sample and the confinement of electrons along z .

By calculating the 1-loop photon propagator in position space, we have been able to localize the interactions of photons with electrons inside graphene, therefore accounting for their “confinement” inside a very thin strip.

One of the main achievements of this study concerns the transmittance function U . The optical properties of graphene cannot be indeed deduced by the sole calculation of the genuine vacuum polarization, would it be in “reduced $QED_{4,3}$ ” [15], because this would in particular neglect all effects due to the confinement of the electron-photon interactions.

The behavior of the refraction index as θ goes to small values has been shown to depend whether an external B is present or not. When $B \neq 0$ there exists a brutal transition at $\theta_{min} \approx \frac{1}{\Gamma}$ below which the quasi-real solution valid above this threshold disappears, presumably (but this is still to be proved rigorously) in favor of a complex solution with large values of n_1 and n_2 (see subsection 7.2). In the absence of B the transition is smooth: n becomes gradually complex with larger and larger values of its real and imaginary components.

Because of the approximations that we have made, and that we list below, we cannot pretend to have devised a fully realistic quantum model. We have indeed:

- * truncated the perturbative series at 1-loop;
- * truncated the expansion of the electron propagator for large B at next-to-leading order;
- * approximated an incomplete β function $F(x) = (-2)^{(-1+x)}\beta(-2, 1-x, 0) \approx \frac{1}{1-x}$, which in particular forget about poles at $p_0^2 = 2neB$ except for $n = 1$; this is however safe for electrons with energy lower than 7 eV , which is certainly the case for graphene through which go photons with energies smaller than 3.5 eV ;
- * chosen a special gauge, the Feynman gauge for the external photons;
- * studied light-cone equations only through their expansions at large $\frac{\sqrt{2eB}}{q_0}$ and small aq_0 .

We can however reasonably pretend to have gone beyond the brutal limit $B \rightarrow \infty$ and to have defined a domain of wavelengths and magnetic fields in which specific expansions and approximations are under control and which are furthermore physically easy to test.

Some comments are due concerning the lack of transversality of the vacuum polarization which arises here, as well as in [10], from the interaction of “quasi-2+1” electrons (in reality 3+1 electrons with p_3 formally vanishing) with 3+1 photons. Lorentz invariance being explicitly broken, one cannot expect anymore the usual gauge invariance of 3+1 QED to hold like in [7].

A specific choice of gauge appears then less chocking, all the more as it is extremely common when making calculations in condensed matter physics to choose the most convenient (Coulomb or Feynman) gauge.

A tantalizing question concerns of course the magnitude of higher order corrections. If 1-loop corrections to the refraction index are large, how can we trust the result, unless all higher orders are proved to be much smaller? At present we have no answer to this. That $\alpha \simeq 2$ inside graphene is already a bad ingredient for a reliable perturbative treatment¹⁵ and, furthermore, the corrections to n do not look like a standard series in powers of α . Comparisons can be made for example with the results obtained in the case of non-confined massive electrons with the effective Euler-Heisenberg Lagrangian [8]. Their equations (2.17)(2.18) show quantum corrections to n proportional to $\alpha \left(\frac{eB}{m_e^2}\right)^2$. In the study of the hydrogen atom [1][2], typical corrections are proportional to $\alpha \frac{eB}{m_e^2}$. In the present study, electrons are massless, and dimensionless factors are built with q_0 in place of m_e . Quantum corrections to the leading $\frac{1}{s_\theta}$ behavior of the index come out proportional to $\left(\frac{\alpha}{\pi}\right)^2 \frac{eB}{q_0^2}$ (see (65)), which is very unusual.

7.2 Going below θ_{min} in the presence of B ; are there also solutions with a large absorption?

We have seen that, as θ decreases, a transition occurs at $\theta \sim \frac{1}{\Gamma} = \frac{q_0}{\sqrt{2eB}}$. The quasi-real solution that we have exhibited for larger angles disappears.

If one considers, below the threshold, at the same $\theta = \frac{\pi}{17}$ the same Fig.7 drawn on a much larger domain for n_1 and n_2 , one gets Fig.12. One solution (at least) occurs for the light-cone equation (82), which corresponds to $n_1 \approx 6.5, n_2 \approx 7$.

¹⁵In the case of the hydrogen atom it was shown in [10] that 2-loop effects are negligible. It is also instructive to look at [16] which show that, in the framework of the Random Phase Approximation and making a 2-loop calculations, graphene, despite a large value of α , behaves like a weakly coupled system. However, in this study, no external magnetic field is present.

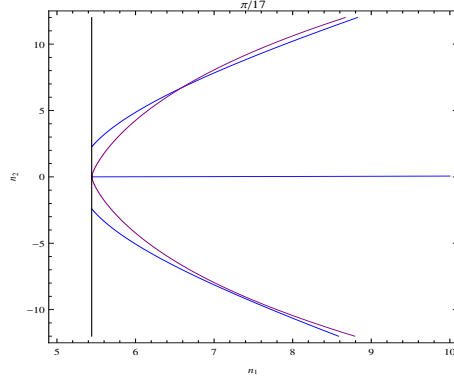


Figure 12: Solutions of the real part (purple) and imaginary part (blue) of the light-cone equation (82) for A_{\parallel}^{μ} at $\theta = \frac{\pi}{17}$ in the presence of B . The black vertical line on the left corresponds to $n_1 = \frac{1}{s_{\theta}}$

This suggests that below θ_{min} , the system goes to a large index with a large absorption. This type of solution is incompatible with the approximations that we have made to find them $|n_2| \ll n_1$ etc, such that drawing a definitive conclusion requires using more elaborate numerical methods. This will be the subject of a forthcoming work. Let us only mention here in addition that such solutions with large index/absorption may coexist, above θ_{min} , with the quasi-real solutions that we have exhibited in this work.

Whether or not total reflection occurs inside graphene at low incidences can only be settled with this more complete study. Notice that, if such a phenomenon occurs, it is at small angle of incidence, again at the opposite of what one is accustomed to with geometrical optics.

A brutal transition like this one may also be the sign of a phase transition at the level of fermions or photons. It has often been evoked that chiral symmetry may get broken inside graphene in the presence of a magnetic field (see for example [17]), and that the photon eventually gets an effective mass (breaking of gauge invariance) should also not be systematically rejected before careful investigations have been done.

7.3 A bridge between Quantum Field Theory, quantum optics and nanophysics

Along this limited study, we have pointed at other potentially interesting phenomena that deserve more detailed investigations: a brutal transition below $\theta = \theta_{min}$ in the presence of B , the eventual existence, in the same conditions, of several types of solutions (including some with large n_1 and n_2), the presence of a “limiting $B = B^m$ ” above which new quantum effects are expected, and, even in the absence of B , some intriguing behavior of the refractive index above $\theta = \theta_{max}$ for $\alpha > 1$.

The issue whether graphene can be safely described in perturbation theory despite a large electromagnetic coupling deserves also, of course, deeper investigations.

The wavelengths of visible light are ~ 1000 times larger than the thickness of graphene. The laws of refraction are therefore not expected to be true. This is confirmed by the existence of solutions to the light-cone equations only satisfying the condition $n \sin \theta > 1$, n being the index inside graphene. Since θ has also been defined as the angle of incidence inside the medium, it is manifestly impossible to satisfy the laws of refraction at its interface with vacuum, which would write $n \sin \theta = 1 \times \sin \theta_{vacuum}$: the l.h.s. is indeed > 1 while the r.h.s. is ≤ 1 .

Graphene in external magnetic field is thus certainly not the realm of geometrical optics, but it could well prove, inversely, a privileged test-ground for the interplay between Quantum Field Theory, quantum optics and nanophysics.

Acknowledgments: it is a pleasure to thank M. Vysotsky for his continuous interest and encouragements.

References

- [1] B. MACHET & M.I. VYSOTSKY: “ Modification of Coulomb law and energy levels of the hydrogen atoms in a superstrong magnetic field”, *Phys. Rev. D* 83 (2011) 025022.
- [2] S.I. GODUNOV, B. MACHET & M.I. VYSOTSKY: “Critical nucleus charge in a superstrong magnetic field: Effects of screening”, *Phys. Rev. D* 85 (2012) 044058.
- [3] M.O. GOERBIG: “Electronic properties of graphene in a strong magnetic field”, *Rev. Mod. Phys.* 83 (2011) 1193, and references therein.
- [4] A.H. CASTRO NETO, F. GUINEA, N.M.R. PEREZ, K.S. NOVOSELOV & A.K. GEIM: “The electronic properties of graphene”, *Rev. Mod. Phys.* 81 (2009) 109.
- [5] J. SCHWINGER: “On Gauge Invariance and Vacuum Polarization”, *Phys. Rev.* 82 (1951) 664.
- [6] W. DITTRICH & M. REUTER: “Effective Lagrangian in Quantum Electrodynamics”, *Lecture Notes in Physics* 220 (Springer-Verlag, Berlin Heidelberg 1985).
- [7] WU-YANG TSAI & T. ERBER: “ Photon pair creation in intense magnetic fields”, *Phys. Rev. D* 10 (1974) 492.
- [8] W. DITTRICH & H. GIES: “Vacuum Birefringence in Strong Magnetic Fields”, *hep-ph/9806417*, *Sandansky 1998, Frontier tests of QED and physics of the vacuum*, 29-43.
- [9] N.M.R. PEREZ, A.H. CASTRO NETO & F. GUINEA : “ Dirac fermion confinement in graphene”, *Phys. Rev. B* 73 (2006) 241403(R).
- [10] S. GODUNOV: “Two-Loop Corrections to the Potential of a Pointlike Charge in a Superstrong Magnetic Field”, *Yad. Fiz.* 76 (2013) 955 [*Phys. Atom. Nucl.* 76 (2013) 901].
- [11] R.R. NAIR, P. BLAKE, A.N. GRIGORENKO, K.S. NOVOSELOV, T.J. BOOT, T. STAUBER, N.M.R. PEREZ & A.K. GEIM: “Fine Structure Constant Defines Visual Transparency of Graphene”, *Science*, vol. 320 (2008) 1308, and references therein.
- [12] WU-YANG TSAI: “Vacuum polarization in homogeneous magnetic fields”, *Phys. Rev. D* 10 (1974) 2699.
- [13] M.E. PESKIN & D.V. SCHROEDER: “An Introduction to Quantum Field Theory”, *Perseus Books* (Reading, Massachusetts) 1995.
- [14] Y.W. SOKHOTSKI: “On definite integrals and functions used in series expansions” *St. Petersburg*, 1873.
J. PLEMELJ: “Problems in the sense of Riemann and Klein”, *Interscience Publishers*, New York, 1964.
- [15] A.V. KOTIKOV & S. TEBER: “Two-loop fermion self-energy in reduced quantum electrodynamics and application to the ultra-relativistic limit of graphene”, *arXiv:1312.2430 [hep-ph]*, *Phys. Rev. D* 89, 065038 (2014).
- [16] J. HOFMANN, E. BARNES & D. SARMA: “Why does graphene behaves as a weakly coupled system ? ”, *arXiv:1405.7036 [cond-mat.mes-hall]*
- [17] V.P. GUSYNIN, V.A. MIRANSKY & I.A. SHOVKOVY: “Dimensional reduction and catalysis of dynamical symmetry breaking by a magnetic field”, *Nucl. Phys. B* 462 (1996) 249-290.